Zhang, Hongxin

HIGH RESOLUTION PHOTOFISSION MEASUREMENTS AND INTERMEDIATE STRUCTURE IN THORIUM-232

City University of New York PH.D. 1986

PLEASE NOTE:

In all cases this material has been filmed in the best possible way from the available copy. Problems encountered with this document have been identified here with a check mark __✓__.

1. Glossy photographs or pages _____
2. Colored illustrations, paper or print _____
3. Photographs with dark background _____
4. Illustrations are poor copy _____
5. Pages with black marks, not original copy _____
6. Print shows through as there is text on both sides of page _____
7. Indistinct, broken or small print on several pages _____
8. Print exceeds margin requirements _____
9. Tightly bound copy with print lost in spine _____
10. Computer printout pages with indistinct print _____
11. Page(s) _____ lacking when material received, and not available from school or author.
12. Page(s) _____ seem to be missing in numbering only as text follows.
13. Two pages numbered _____. Text follows.
14. Curling and wrinkled pages _____
15. Dissertation contains pages with print at a slant, filmed as received __✓__
16. Other _____

_____

_____

University
Microfilms
International

HIGH RESOLUTION PHOTOFISSION MEASUREMENTS

and

INTERMEDIATE STRUCTURE IN ^{232}Th

HONGXIN ZHANG

A dissertation submitted to the Graduate Faculty in Physics in partial fulfillment of the requirements for the degree of Doctor of Philosophy, the City University of New York.

1986

This manuscript has been read and accepted for the Graduate Faculty in Physics in satisfaction of the dissertation requirement for the degree of Doctor of Philosophy.

2/11/1986
Date

Chairman of Examining Committee

2/14/86
Date

Executive Officer

Prof. L.S. Celenza (Brooklyn College)

Prof. P.M. Lesser (Brooklyn College)

Prof. Carl Shakin (Brooklyn College)

Prof. J. Ullman (Lehman College)

Supervisory Committee

The City University of New York

Abstract

HIGH RESOLUTION PHOTOFISSION MEASUREMENTS

and

INTERMEDIATE STRUCTURE IN ^{232}Th

by

Hongxin Zhang

Adviser: Professor Henry Lancman

The photofission cross section of ^{232}Th was measured in the energy range 5.8 - 12 MeV with an average photon energy resolution of 600 eV. The gamma rays, variable in energy, were obtained from narrow (p,γ) resonances in various nuclei. Intermediate structure was observed at subbarrier excitation energies. The average spacing of photofission resonances provided the first relatively direct determination of the energy of the second minimum of the fission barrier, relative to the ground state. The measured fission probability and various properties of the intermediate structure were found to agree with calculated values based on a double humped fission barrier. The features of this barrier, a rather high first hump and a deep secondary well, are quite different from the predictions of current theoretical barrier calculations.

ACKNOWLEDGEMENTS

I would like to express my deep appreciation to my research adviser, Professor Henry Lancman, for suggesting the idea of searching for intermediate structure at subbarrier excitation energies of ^{232}Th, in order to study the properties of its fission barrier. I am also grateful for his continuous advice during the course of this work.

I also wish to thank Prefessor Carroll C. Trail, the former director of this laboratory, and Professor Peter Lesser, the current director, for suggestions helpful in obtaining the large proton beam currents, which were very important in this work.

I am indebted to M.R. Stolfo and K. Davenport for their help with the software for the scanner.

Many members of the laboratory staff have contributed their efforts to these experiments. Among them, Donald King, William Stuber, Sol Coltun, Martin Berman, and Ira Senzon deserve particular credit for their useful advice and helpful assistance. Special thanks are due to Sol Coltun for his help in building the automatic sparker of Kimfol film. I am also grateful to P. Punyasena for help in the processing of the film.

CONTENTS

LIST OF TABLES

LIST OF ILLUSTRATIONS

CHAPTER I

CHAPTER II

CHAPTER III

CHAPTER IV

INTRODUCTION AND SUMMARY

The properties of the fission barrier of thorium isotopes and other light actinides have been given much attention in recent years because agreement between the theoretical and experimental results is far from satisfactory for these nuclei.[1] This is in contrast to the situation in heavier actinides where agreement with the predictions based on the double humped fission barrier model is very good.[1,2,3] The most pronounced difference between theory and experiment has existed in the cases of ^{231}Th and ^{233}Th. The observation[5] of undamped vibrational resonances in the ^{230}Th(n,f) and ^{232}Th(n,f) cross sections at excitaion energies above 5.8 MeV has implied,within the confines of the double hump model,an inner barrier height $E_A \approx$ 6MeV and a secondary well with a minimum at $E_{II} \approx$ 4.5 MeV. On the other hand ,theoretical calculations have yielded[4] $E_A \approx$4.5 MeV and $E_{II} \approx$2.5 MeV.

A solution to this difficulty was proposed by Moller and Nix,[4] who obtained in their calculation for light actinides a low inner barrier and a shallow third well at the deformation of the outer barrier by taking into account γ deformation and mass asymmetry. Evidence of the existence of a third well has been found in the recent high energy resolution measurements in ^{230}Th(n,f), and ^{232}Th(n,f). Fine structure observed within the undamped vibrational resonances in these reactions has been interpreted as rotational states built on vibrational states in the third well.[8] However ,it has been shown by Lynn[9] that the observed structure could also result from the coupling of single particle and vibrational motion. Data obtained in high resolution measurements of structure at subbarrier excitation energies would shed light on this question.Unfortunately such data have not been available in abundance.

The present thesis work is a high resolution photofission measurement on ^{232}Th. Its primary aim is a search for structure at subbarrier energies. Photofission has long been recognized as a promising method to investigate the fission barrier. The entrance channel, predominantly electric dipole photon absorption, is well understood. As a result of the selective absorption, only states with a limited range of angular momenta are inolved in the process. In the even even nuclei these are predominantly 1^- states. This makes identification of spins and parities of fission barriers much easier than in the case of particle induced fission.

The experimental setup is described in detail in the main body of this thesis. Briefly, a collimated proton beam of average current 150 μA strikes a water cooled target mounted in a vibrating target assembly(Fig. 1 of Chapter II). The emerging gamma rays are allowed to fall on sandwiches of 30 mg/cm^2 thick thorium or uranium foils in close contact with 8 μm Kimfol films serving as fission track recorders. The sandwiches are placed on a cylinder coaxial with the proton beam(Fig.1 of Chapter IV). The energy of the gamma rays varies with the angle relative to the proton beam as a result of the Doppler shift. The average photon energy dispersion is 200 eV/degree. A typical photon energy range from a resonance is 20 keV.

The measured photofission cross section at subbarrier excitation energies in ^{232}Th shows prominent resonances, which are interpreted as representing intermediate structure. The average resonance spacing yields E_{II}= 2.8 MeV. This is the first relatively direct determination of this quantity. Details of other results obtained at subbarrier excitation energies and their interpretation are given in[12] Chapter III. These

results also suggest the E_A is about 6 MeV, a value which is consistent with the broad resonance[6,7] at an excitation energy of about 6 MeV, but is quite different from the predictions of the current theoretical calculations.[4,13,14] Since it is impossible to determine accurately the remaining fission barrier parameters from the intermediate structure only, the measurements were extended to photon energies up to 12 MeV. The results given in Chapter IV allow us to determine the complete set of fission barrier parameters by fitting both, the measured fission probability, and the observed structure. It turns out that the data can be adequately interpreted on the assumption of a double humped barrier shape but a shallow third well can not be excluded.

The complete set of parameters of the fission barrier of ^{232}Th, for $J^{\pi}=1^-$, K=0,1 obtained from the present measurements is listed in Table I of Chapter IV. The remaining question concerns the existence of the shallow third well at the deformation of the outer barrier. To answer it one needs to search for resonances $\sim$ 30 keV wide at an excitation energy $\sim$ 6 MeV, with photons having an energy resolution $\sim$2 keV. Such narrow resonances could represent the undamped vibrational states in the shallow well. In principle, this can be done by using photons from p(heavy ion, γ) resonances.

High energy resolution photofission measurements on ^{238}U have been also simultaneously carried out in the photon energy range 5.8 - 12 MeV. The data is still being processed and will be published soon. The cross sections are listed versus energy in Appendix I.

References

1. S. Bjornholm and J.E. Lynn, Rev. Mod. Phys. 52 (1980) 725.

2. V.M. Strutinsky, Nucl. Phys. A95 (1967) 420.

3. V.M. Strutinsky, Nucl. Phys. A122 (1968) 1.

4. P.Moller and J.R.Nix,in Proceedings of the Third Int. Symp.on the Phys.and Chem.of Fission , Rochester 1973 (IAEA,Vienna,1974), Vol. 1, P.103.

5. J.Blons, C.Mazur, D.Paya, M.Ribrag, and H.Weigman, Phys. Rev. Lett 41 (1978) 1282.

6. P.A.Dickey and P.Axel ,Phys.Rev.Lett.35 (1975) 501.

7. J.W.Knowles, W.F.Mills, R.N.King, B.O.Pich, S.Yen, R.Sobie, L.Watt, T.E.Drake, L.S.Cardman, and R.L.Gulbranson, Phys. Lett. 116B (1982) 315.

8. J.Blons,C.Mazur,D.Paya,M.Ribrag and H.Weigmann,Nucl. Phys.A414 (1984) 1.

9.J.E.Lynn,J.Phys.G:Nucl.Phys.9 (1983) 665.

10.H.X.Zhang, T.R.Yeh,and H.Lancman, Nucl. Intr. & Meth. 214 (1983) 391.

11.H.X.Zhang, T.R.Yeh ,and H.Lancman, Nucl. Intr. & Meth. A239 (1985)459.

12.H.X.Zhang,T.R.Yeh,and H.Lancman,Phys.Rev.Lett.53 (1985) 34.

13.J.Dudek,W.Nazarewicz,and A.Faessler,Nucl.Phys.A412 (1984) 61.

14.W.M.Howard and P.Moller,Atomic Data and Nucl. Data Tables 25 (1980) 219.

AUTOMATIC SCANNING OF SOLID STATE NUCLEAR TRACK DETECTORS AT LOW TRACK DENSITY

H.X. Zhang, T.R. Yeh, and H. Lancman
Physics Department, Brooklyn College of CUNY,
Brooklyn, N.Y. 11210, U.S.A.

ABSTRACT

A device for scanning large areas of Kimfol fission track detectors is described. It is being used in photofission experiments where $\sim 10^4$ cm^2 of film per run have to be handled. The tracks are first enlarged by etching and sparking. The film is then scanned by a high resolution Vidicon camera and the x and y coordinates of each track are stored in a computer. A typical scanning speed is 10 cm^2/sec. The counting efficiency is close to 100%.

1. Introduction

Solid state track detectors have found extensive use in fields ranging from nuclear physics to archeology.[1] In many applications a very valuable characteristic of these detectors is their position sensitivity. A serious disadvantage is the often encountered necessity to carry out the scanning and position measurements of the tracks manually. Techniques for accurate automatic scanning which employ an optical microscope coupled to a television camera have been developed[2-5] mainly for handling detectors of small area and high track density (10^3-10^4 tracks/cm^2). Methods based on spark counting[6,7] have been used for the determination of the total number of tracks over large areas of thin film. They are not suitable however for accurate measurements of the positions of the tracks.

Photofission measurements, which we have been carrying out[8] using thin polycarbonate Kimfol films as fission fragment detectors, require scanning of very large areas of film ($\sim 10^4$ cm^2 per run) with a high accuracy in the determination of the position of each track.

The gamma rays in our measurements are obtained from various (p, γ) resonances in light nuclei. Owing to the Doppler shift, the energies of these gamma rays vary continuously as a function of the emission angle θ relative to the proton beam. Multilayer sandwiches of foils containing

fissile nuclei and Kimfol films are placed on a cylindrical surface having the proton beam as its axis. Fission events induced by photons of energy between $E(\theta)$ and $E(\theta+\Delta\theta)$ lie on a strip of film determined by the intersection of the cylinder with cones of vertex angles θ and $\theta+\Delta\theta$ originating at the proton target. A typical energy dispersion is of the order of 200 eV/degree , which in the presently used geometry corresponds to ~ 200 eV per 1 mm wide strip. For scanning, the tracks produced by the photofission fragments in the film are made visible to the naked eye by first etching the film and then passing it through a set of spark gaps.[9] Sparking enlarges the tracks turning them into tiny holes in the film. In the process, information contained in the properties of the tracks is destroyed. However, since the fission fragments enter the film at a wide range of angles and the foil from which they emerge is thick in comparison to the fragment's range, this information would not be particularly illuminating.

2. The scanner

The scanner, shown schematically in Fig. 1, employs a Hamamatsu C1000-00 vidicon camera equipped with a Nikon 55 mm f/3.5 Micro-Nikkor lens and interfaced to a PDP-11/20 computer. Designed for precision image analysis this camera is characterized by very low distortions and high stability.

Because of the difficulty in handling the 8 μm Kimfol film, Xerox copies are used for scanning. The paper copy of the film on which the holes representing tracks appear as dark dots is placed on a translational stage facing the camera and advanced manually in discreet steps. A monitor

is used to control the lighting conditions, lens setting and position of the film. Scanning can be done with, in order of increasing resolution, 256, 512 or 1024 lines in both the x and y directions. The address signals are processed to determine the coordinates of the center of each dot, which are then stored in the memory of the computer.

To be processed, the size of a dot has to fall within limits set in the program to ensure that various forms of background such as dust, scratches, creases and other extraneous marks on the film or the paper are not counted as valid data. These limits are determined by the conditions used in developing the film. The background can also be discriminated against on the basis of the gray level.

3. Efficiency

The scanning efficiency is defined as the ratio of the total number of dots counted by the camera to the total number of dots counted by eye on the same film. An efficiency close to 1.00 can be obtained for several sets of conditions as can be seen from Fig. 2, where the efficiency is plotted against the threshold setting that determines the gray level below which the video signal is accepted. The four curves correspond to different scanning resolutions and different minimum dot sizes N_{min}, the smallest number of lines across a dot, in the x or y direction, below which the dot will not be counted by the program. The upper limit on the dot size has been kept at $N_{max}=32$ lines.

The different slopes on the left side of each efficiency curve and their different onset thresholds reflect the gray level distribution across a single dot and the dots' size distribution. The onset of the rapid increase at the

right end of each curve indicates acceptance of background. The plateau for resolution 512, N_{min}=2 is longer than the one for resolution 1024 as a consequence of the small size of the average background dot. In the remaining two counting conditions background is caused by accidental coincidence of several background dots in the right spatial configurations. The number of such dots necessary for acceptance is higher in the case of resolution 512, N_{min}=3 than for resolution 256, N_{min}=2. The plateau in the latter case is therefore shorter.

4. Size Distribution and overlap

Fig. 3 shows the number of dots as a function of N (the smaller of N_x and N_y) determined with a gray level threshold set at the midpoint of the plateau for resolution 256. The distribution of dots representing fission tracks is centered at N=8.5 and is well separated from the background which increases rapidly for small values of N. The magnitude of this separation can be varied by changing the sparking conditions. An important consideration in choosing the latter is dot overlap.

The probability of overlap increases with the size and density of the dots. Because of their irregular shapes (the result of sparking) two or more overlaping dots can not be distinguished from a single one and are counted as such by the program. The typical track density encountered in our experiments is $\sim$5 per cm^2. Given the average size of a dot this leads[10] to a correction $\lesssim$3% in the number of counts. Making the dots smaller by changing the sparking conditions would reduce the overlap correction, but it would also make discrimination against background less certain. The average size of a dot is

chosen to minimize the combined correction for overlap and background.

5. Reproducibility, accuracy, and scanning speed

The counting rate reproducibility of the camera was obtained by scanning the same copy of a film a number of times over a 12 day period with the copy left in place and the scanner turned on and off once a day. The counts were found reproducible within a standard deviation of 0.6%. This deviation from perfect reproducibility is caused by cases of marginal overlap where spatial resolution is very sensitive to the stability of threshold, illumination, etc.

The counting reproducibility of the whole scanner, including camera and positioning device, was obtained by repeatedly placing, scanning, and removing the same copy of a film. The counts were found reproducible within a standard deviation of 1%.

For the dot sizes used in our work the position reproducibility of the camera over a time interval of 10 hours is within 0.5 of a scanning line. The overall position reproducibility is affected by the accuracy of mounting the film on the translational stage and the alignment of the stage in its various positions relative to the camera. It was found that the coordinates of a dot are reproducible within a standard deviation of one scanning line at resolution 512. Good position reproducibility is important for preserving the energy resolution of the gamma rays in our experiments.

Another factor affecting the energy resolution is due to image distortions. These distortions caused mainly by nonlinearity of the camera's response do not exceed 1% for the Hamamatsu C1000 camera.

Because of the large areas of film which have to be analyzed in our experiments, the speed of scanning is an important characteristic of the

instrument. It depends on the track density and scanning resolution. A typical value in our measurements is 10 cm^2/sec.

6. A sample spectrum

Figure 4 shows a spectrum of photofission fragments counted over strips of film ΔX corresponding to gamma ray energy intervals of 100 eV. The combined errors in determining the dot position translate into a gamma ray energy uncertainty of $\sim$ 50 eV. This is three times smaller than the average gamma ray energy resolution which varies somewhat in magnitude across the spectrum. The counting rate errors of the scanner are negligible in comparison with the statistical errors shown by the vertical bars.

7. Conclusions

At very low densities of fission tracks, and when the desired information is limited to the number of tracks and their positions, scanning is greatly facilitated by enlarging the tracks and allowing the camera to examine large areas of the detector at one time. Background discrimination, a serious problem in automatic scanning[10], becomes straightforward as a result of the enlargement; however, overlap corrections also increase.

The device described here provides, apart from scanning speed, an accuracy in counting and position determination that is difficult to achieve by manual scanning.

The authors would like to thank M. R. Stolfo and K. Davenport for their help with the computer program. Thanks are also due to Dr. M. Ismail for his assistance at the initial stage of these investigations. This work was supported by the U. S. Department of Energy and by the PSC-BHE Faculty research Award Program of CUNY.

References

1. R.L. Fleischer, P.B. Price and R.M. Walker, Nuclear Tracks in Solids (University of California Press, 1975).
2. J.U. Schott, E. Schopper and R. Staudte, Nucl. Instr. and Meth. 147 (1977) 63.
3. D. Azimi-Garakani and J.G. Williams, Nucl. Instr. and Meth. 147 (1977) 69.
4. S. DiLiberto and P. Ginobbi, Nucl. Instr. and Meth. 147 (1977) 75.
5. W. Abmayr, P. Gais, H.P. Paretzke, K. Rodenacker and G. Schwartzkopf, Nucl. Instr. and Meth. 147 (1977) 79.
6. K. Becker et al. Nucl. Instr. and Meth. 124 (1975) 557.
7. B.H. Patrick and E.M. Bowey, Nucl. Instr. and Meth. 120 (1974) 245.
8. T.R. Yeh and H. Lancman, IEEE Trans. Nucl. Sci. NS-28 (1981) 1289.
9. T.R. Yeh and H. Lancman, Nucl. Instr. and Meth. 179 (1981) 141.
10. R. Gold and C. Cohn, Rev. Sci. Instr. 43 (1972) 18.

Figure Captions

Fig. 1. Schematic diagram of the scanner.

Fig. 2. Scanning efficiency as a function of the gray level threshold setting for several values of the minimum acceptable dot size and scanning resolution.

Fig. 3 The size distribution of the dots. N represents the number of lines across a dot at resolution 1024. Scanning was done at 0.05mm per line.

Fig. 4. A spectrum of photofission fragments of ^{238}U in the photon energy range from 6069 to 6076 keV. The Ep = 2037 keV resonance in the $^{42}Ca(p,\gamma)$ reaction was used to produce the photons. The dispersion due to the Doppler shift is in this case 164 eV/degree at $\theta = 90^{o}$.

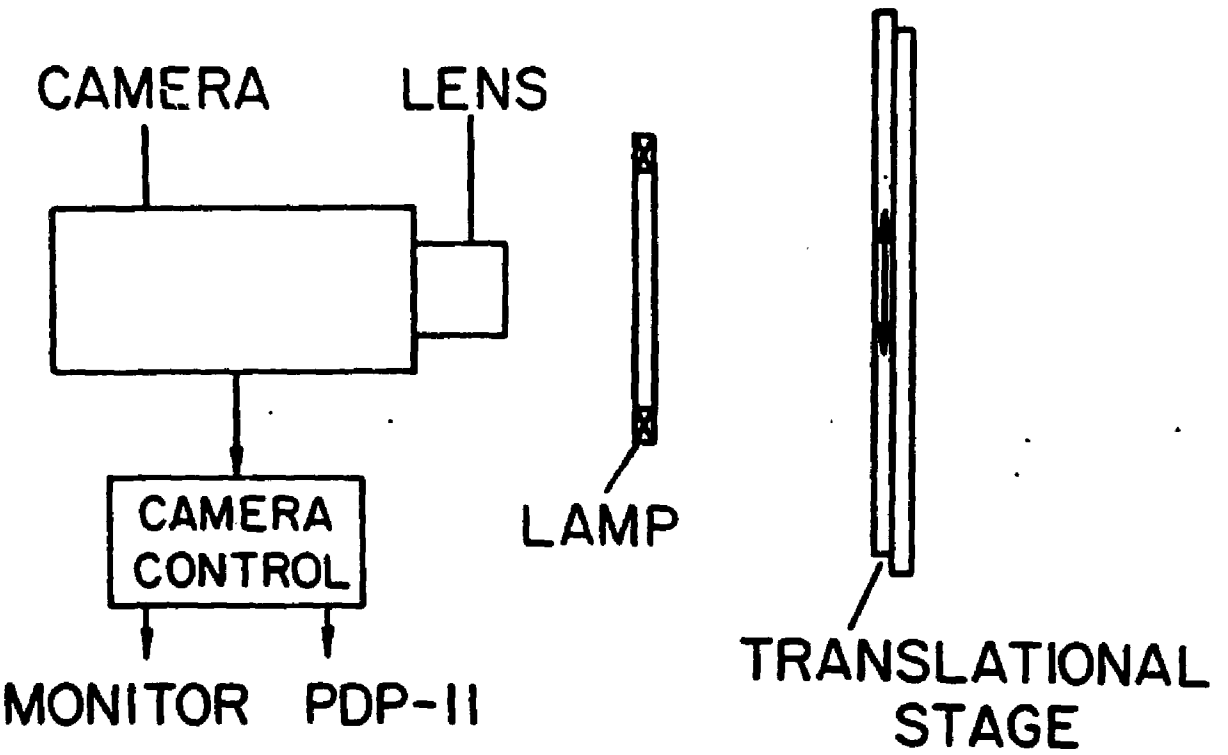
CAMERA
LENS
CAMERA CONTROL
LAMP
MONITOR
PDP-11
TRANSLATIONAL STAGE

Fig. 1

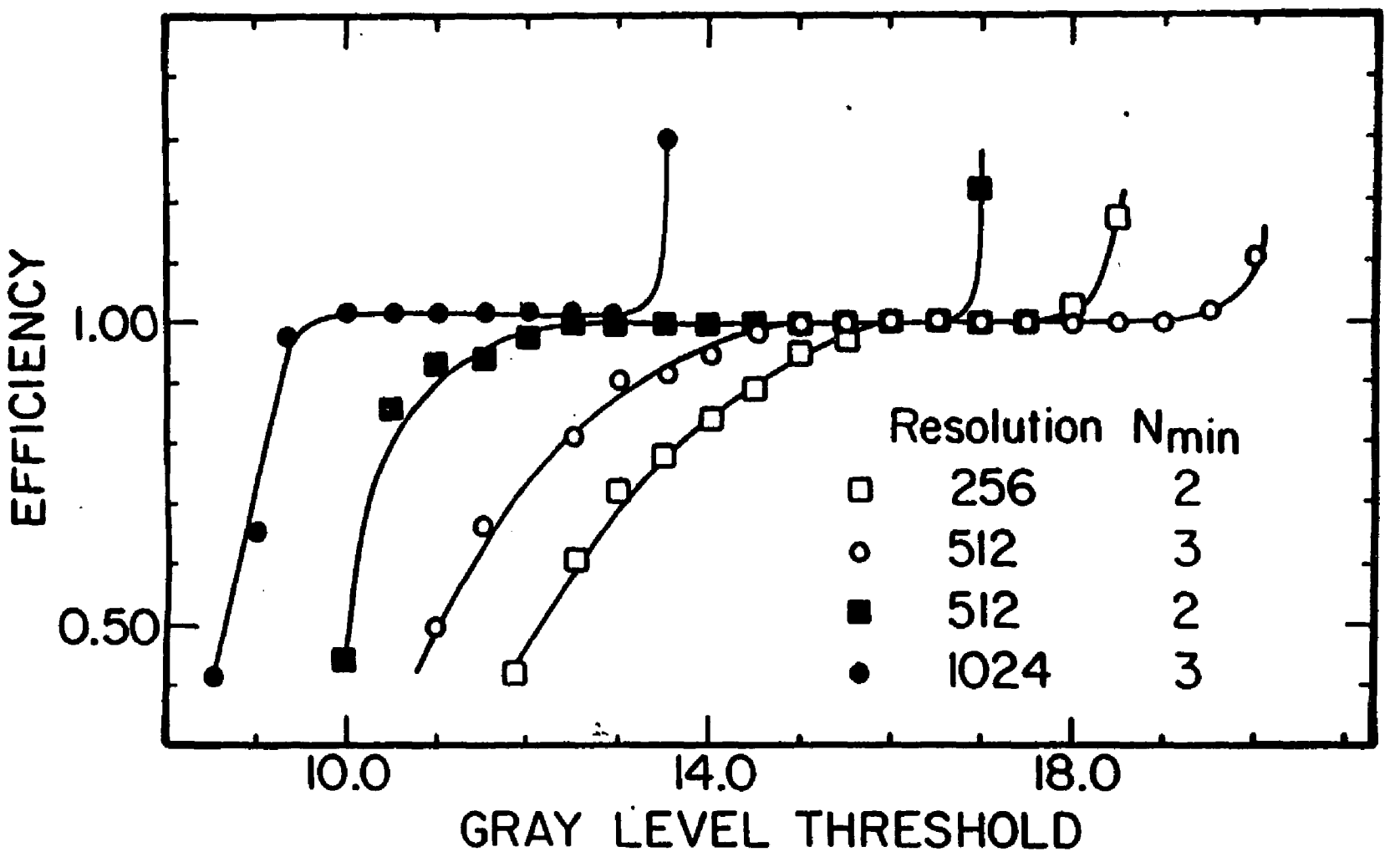
EFFICIENCY
1.00
0.50
10.0
14.0
18.0
GRAY LEVEL THRESHOLD
Resolution Nmin
256 2
512 3
512 2
1024 3

Fig. 2

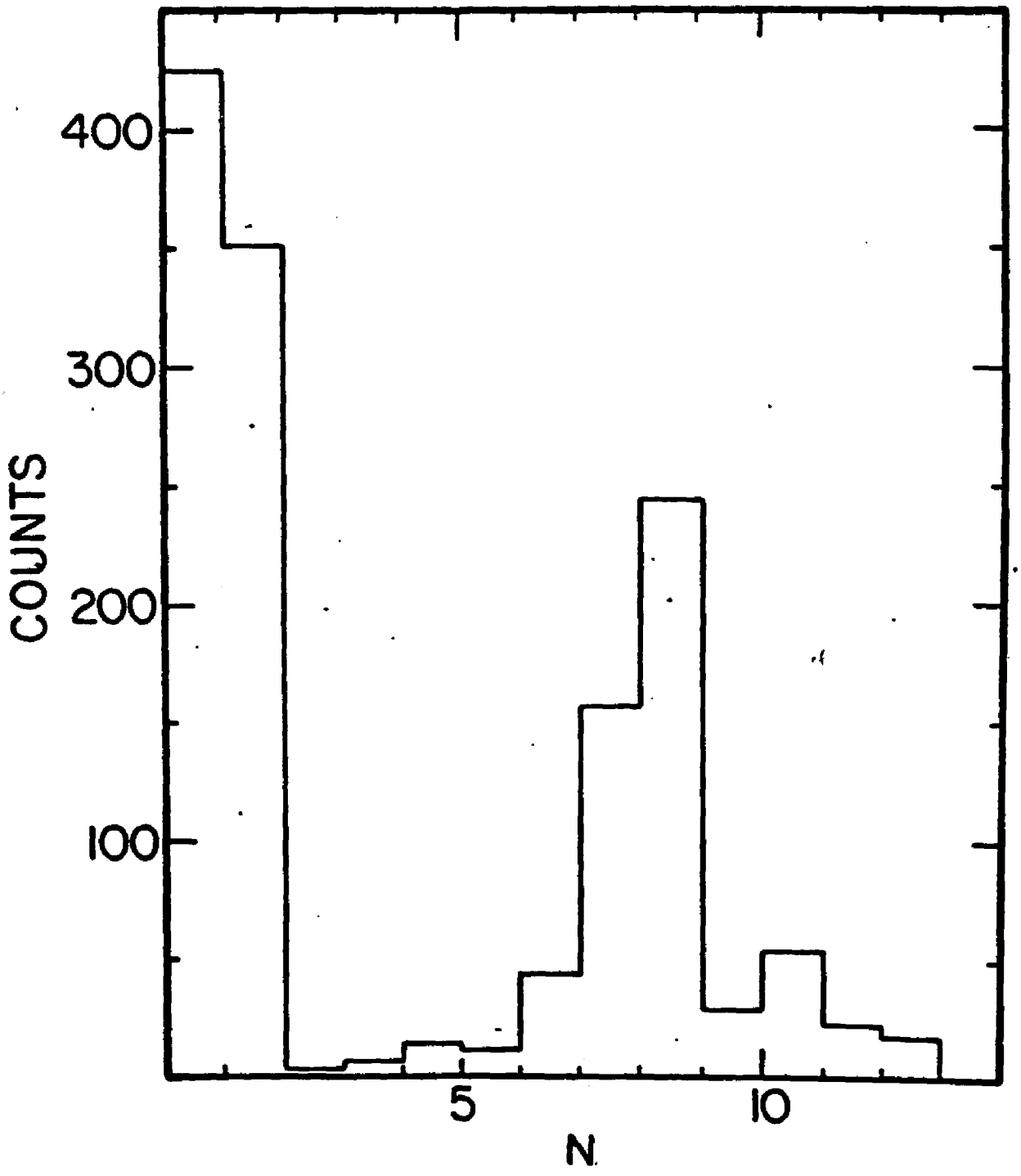

Fig. 3

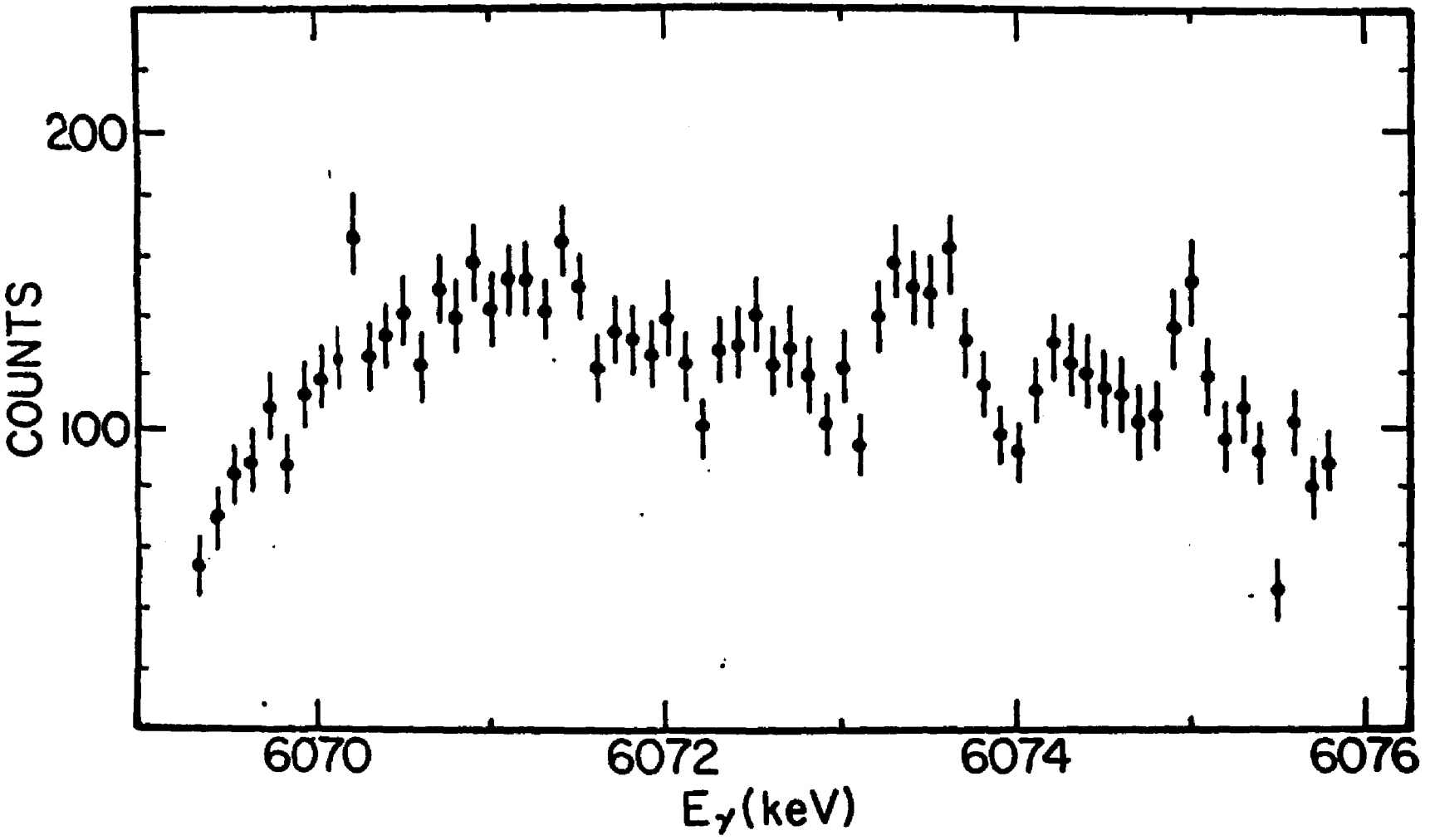

Fig. 4

A VIBRATING TARGET ASSEMBLY FOR INTENSE ION BEAMS

H. X. ZHANG AND H. LANCMAN

PHYSICS DEPARTMENT, BROOKLYN COLLEGE OF CUNY
BROOKLYN, N.Y. 11210

Abstract

A high power vibrating target assembly was designed for work with well-collimated intense proton beams. The water-cooled target vibrates in two mutually perpendicular directions at different frequencies. It is shown that for many target materials power dissipation up to 0.5 kW/cm^2 can be tolerated over long time intervals.

A vibrating target assembly was designed as part of a facility[1] for generating monochromatic gamma rays of variable energy at our 3.75 MeV Dynamitron Accelerator.

The gamma rays are obtained from selected (p,γ) resonances in various light nuclei. Their energies vary due to the Doppler shift within a typical range of 10-30 keV. Because the cross sections of the (p,γ) reaction are low it is necessary to employ a high proton beam current, up to 2 mA is available from the Dynamitron, to assure an adequate gamma ray yield. At the same time it is desirable to have a very small cross sectional area of the beam on target in order to preserve the excellent energy resolution of the gamma rays, limited in principle, at a fixed angle to the proton beam, by the natural width of the particular (p,γ) resonance, if thermal Doppler broadening is neglected. The lifetime of the target under these conditions can be increased many fold if it is moved continuously relative to the beam so that the dissipated power is distributed over a large area.

An often used design accomplishes this by rotating the target.[2] The power dissipation capabilities of commercially available rotating target assemblies are rated in the kW range. Such assemblies have typically been used for the generation of intense neutron fluxes. For the present work, in which many, often quite expensive, target materials have to be used, a rotating target is not the best solution of the power dissipation problem because such a design does not allow for an efficient use of the target area.

A compact design in which the target, driven by a system of coupled gears, describes Lissajous figures in the plane perpendicular to the

proton beam was described by Hoffman et al.[3] Although in this case the beam is distributed over the whole target, the spreading is not uniform since the sinusoidal motion along the x and y directions makes the beam spend more time per unit area at the periphery of the target than in its middle.

Our design is shown schematically in Fig. 1. The target chamber is mounted at the end of a bellows and supported by a translational stage. The stage is driven in the horizontal direction by an electromagnetic vibrator,[4] while its support is moved up and down by another vibrator. Sawtooth waves superimposed on adjustable d.c. potentials are applied to each vibrator so that the latter's frequencies, amplitudes, and equilibrium positions can be varied independently. At low frequencies, the vibrators' displacements depend linearly on time with good accuracy so that the target chamber follows a triangular wave pattern in both its horizontal and vertical directions. This is shown in Fig. 2, where the frequencies of the x and y vibrations are 0.45 Hz and 0.1 Hz, respectively. As can be seen, the beam covers the selected area of the target with great uniformity. The maximum amplitude in the present system is 12 mm. The electroformed nickel bellows[5] are designed to withstand 10^8 vibrations at this amplitude.

Four beam sensors are placed 90° apart around the cylindrical target chamber in a plane parallel to the target and 10 mm from it. A negative bias of 10 V is applied to the sensors to protect them from electrons ejected by the target. The currents from the sensors provide information on the position of the beam relative to the target. They are used to control the amplitude, and equilibrium position of the chamber during long runs.

The target material is deposited on a 0.25 mm tantalum foil. The back of the foil is continuously cooled by chilled water flowing under pressure of 40 psi at a rate of 10 liters per minute.

Figure 3 shows the yield of the 9.365 MeV photons from the 2.488 MeV resonance in ^{27}A (p,γ) as a function of time for several values of power dissipation per cm.^{2} The targets were 50 μm thick and were obtained by evaporation in vacuum. At a power density of 2.5 kW/cm^2 the yield decreases rapidly, indicating fast target deterioration (leading to puncture). At densities $\leq$ 0.7 kW/cm^2 the yield remains practically constant over a long time interval. Although different target materials behave differently, a limit of 0.5 kW/cm^2 for long range yield stability is applicable to most targets used in (p, γ) work.

The effective target area in the present design is 3 cm^2 which provides a power dissipation capability under conditions of stable yield of 1.5–2 kW. This is sufficient for generating photon beams of adequate intensity for many photonuclear experiments.

The authors would like to thank Dr. T. R. Yeh for his help at the early stages of this work. This work was supported by the USDOE and the PSC-BHE Research Award Program of CUNY.

References

1. H. X. Zhang, T. R. Yeh and H. Lancman, Phys. Rev. Lett., 53 (1984) 34.

2. E. H. Woodburn, M. Barette, J. L. Foster, Jr. and G. Lamoureux, Nucl. Instr. and Meth. 109 (1973) 561.

3. D. Hoffmann, G. Sobtotta, K. Becker, H. Genz, A. Richter and G. Schrieder, Nucl. Instr. and Meth. 118 (1974) 321.

4. Vibration Test Systems, Aurora, Ohio 44202, U.S.A.

5. Servometer Corporation, Cedar Grove, New Jersey 07009, U.S.A.

Captions to Figures

Fig. 1. Schematic diagram of the target assembly.

Fig. 2. Trace of the proton beam on the target at $\nu_x = 0.45$ Hz and $\nu_y = 0.1$ Hz. Departures from linearity at the end of each displacement have been neglected.

Fig. 3. Time dependence of the yield of the 9.365 MeV gamma rays from the 2.49 MeV resonance in $^{27}Al(p,\gamma)$ for two values of power dissipation density.

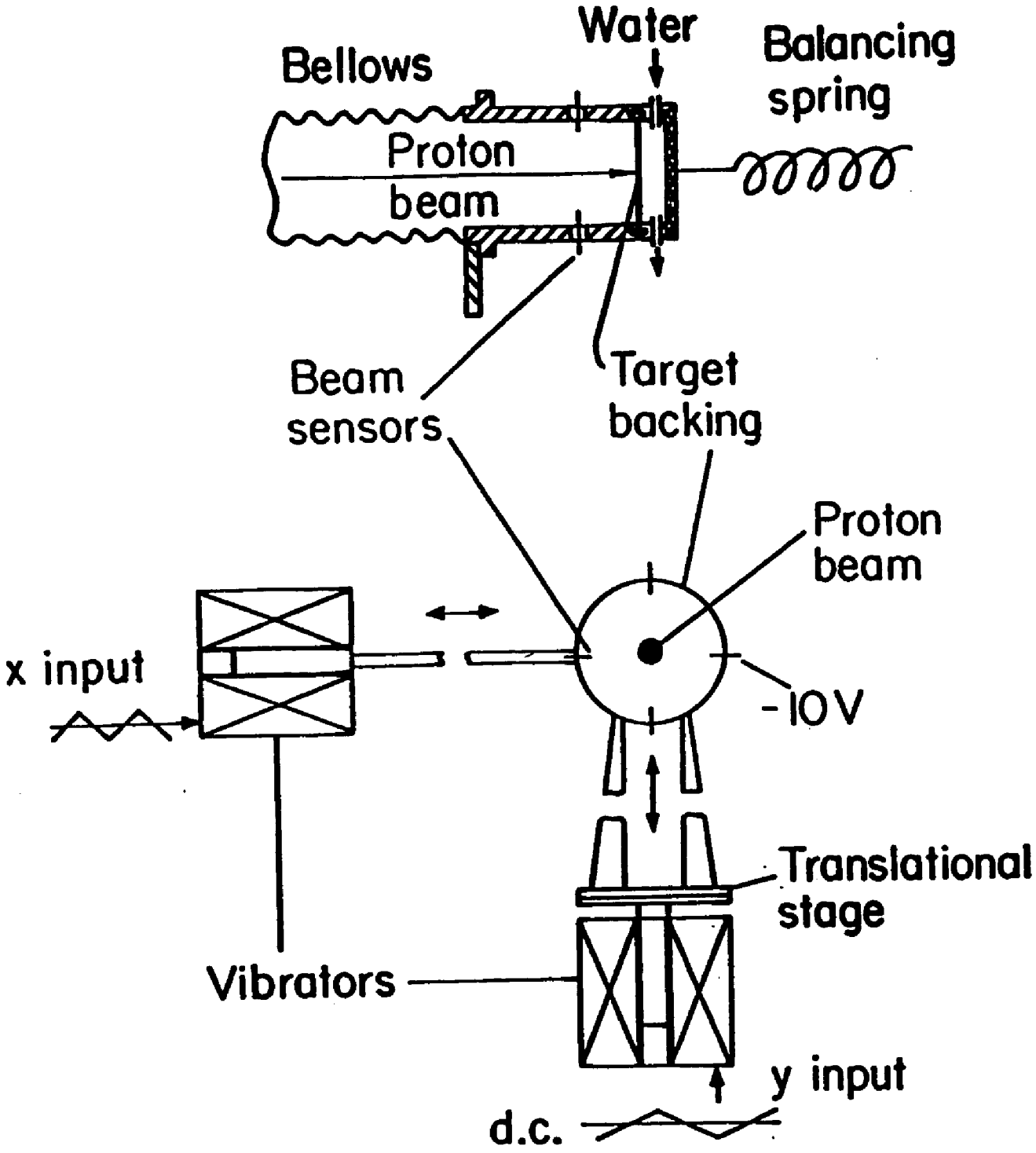
Water
Bellows
Balancing spring
Proton beam
Beam sensors
Target backing
Proton beam
x input
-10V
Translational stage
Vibrators
y input
d.c.

Fig. 1

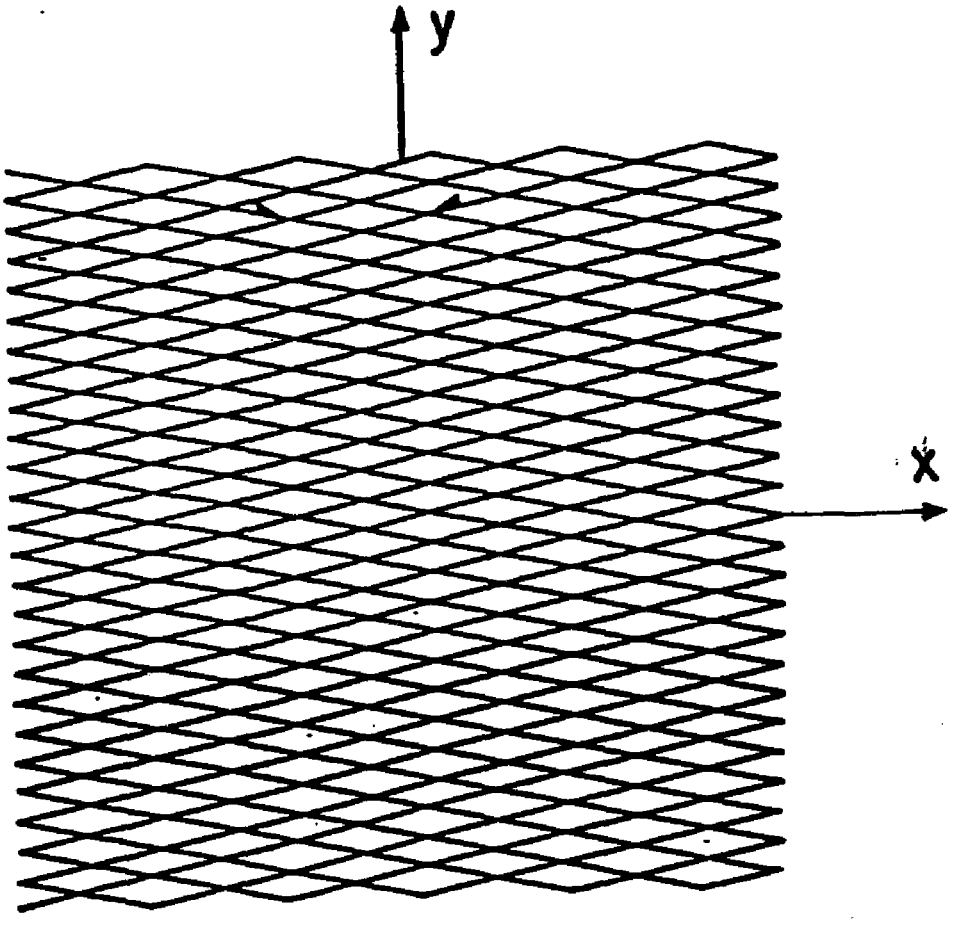

Fig. 2

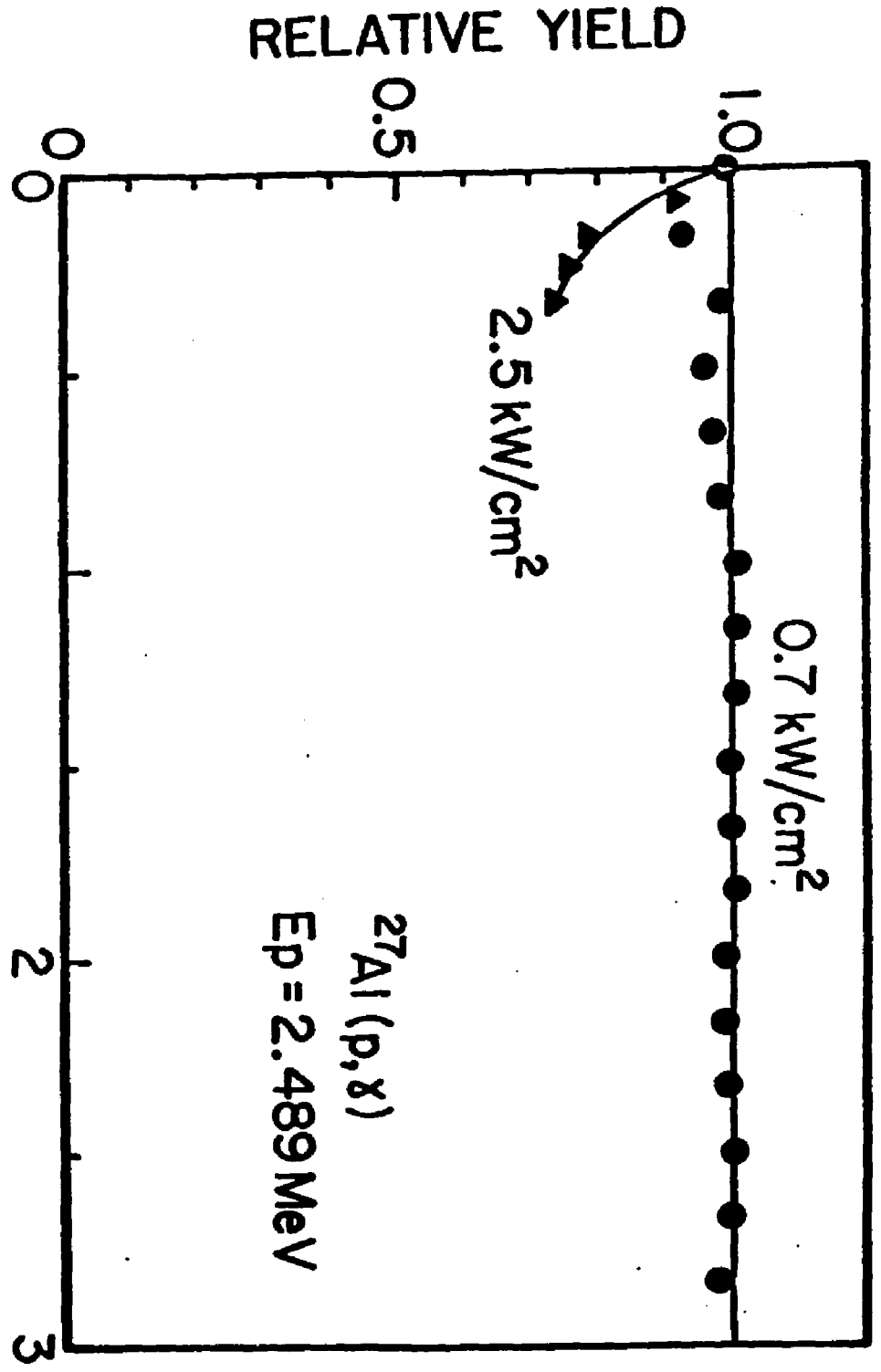
RELATIVE YIELD
0
0.5
1.0
0.7 kW/cm²
2.5 kW/cm²
27Al (p,γ)
Ep = 2.489 MeV
TIME (hr)
2
3

Fig. 3

Intermediate Structure in the Photofission Cross Section of ^{232}Th

H.X. Zhang, T.R. Yeh and H. Lancman
Physics Department, Brooklyn College of CUNY
Brooklyn, N.Y. 11210

Abstract

Intermediate structure has been observed in the photofission cross section of ^{232}Th measured with a photon energy resolution $\lesssim$500 eV. The gamma rays, variable in energy, were obtained from the (p, γ) reaction on several nuclei. The average spacing of the observed photofission resonances at an excitation energy of 6.16 MeV is 1.6 $\pm$ 0.4 keV. The average areas of the resonances are compared with theoretical expectations for a double-humped and a triple-humped barrier.

PACS numbers: 25.85.Jg

The properties of the fission barriers of actinide nuclei have been, in large measure, derived from studies of structure in the fission cross section at subbarrier excitation energies.[1] Much attention has been given to the question of the shape of the barrier in thorium isotopes, where barrier calculations have been in disagreement with experimental data.[1] The existence of undamped vibrational resonances in the ^{230}Th(n,f) and ^{232}Th(n,f) cross sections at excitation energies above 5.8 MeV has implied, within the confines of the double-hump model, an inner barrier height $E_A \gtrsim 6$ MeV and a secondary well with a minimum at $E_{II} \gtrsim 4.5$ MeV. On the other hand, theoretical calculations, generally successful in predicting barrier heights for heavier actinides, have yielded[2] $E_A \simeq 4$ MeV for thorium isotopes. This discrepancy has been known as the thorium anomaly.

A solution was suggested by Möller and Nix[2] who obtained in their calculations for light actinides a low inner barrier and a shallow third well at the deformation of the outer barrier. Experimental evidence for such a triple-humped barrier has been provided[3] by investigations of the structure within the vibrational resonances in ^{231}Th and ^{233}Th.

Subbarrier structure has been observed in many nuclei, mainly in high resolution measurements of neutron induced fission. However, such measurements cannot be done when the neutron separation energy exceeds the height of the barrier. This is the case in ^{232}Th, a nucleus whose barrier structure is expected[2] to be similar to that of its neighbors. A way to reach subbarrier energies in ^{232}Th is provided by photofission.

Photon-induced fission takes place only from states which can be reached by electric dipole and, with a much smaller probability, electric

quadrupole excitations. This makes identification of spins and parities much easier than in the case of particle induced fission where a much wider range of angular momenta is possible.

The main difficulty in photofission experiments is in obtaining monochromatic photons of variable energy and adequate intensity. Compton scattered as well as direct gamma rays from slow neutron capture, bremsstrahlung, and tagged bremsstrahlung have been used.[4,5] The last technique in its improved version provides an energy resolution of 12-14 keV for 6 MeV photons.

In this paper we present results of measurements of the photofission cross section of ^{232}Th carried out with a photon energy resolution <500 eV. These measurements for the first time clearly reveal narrow intermediate structure resulting from the excitation of compound states in the second well of the fission barrier of ^{232}Th. Similar structure has been found in neutron and charged particle induced fission of various nuclei.[1] Intermediate structure has not been observed before in photofission.

A novel technique in which the photons are obtained from resonances in the (p, γ) reaction has been employed.[6] The experimental setup is shown schematically in the inset of Fig. 1. A collimated proton beam of average current ~ 150 μA from our Dynamitron strikes a water-cooled target mounted in a vibrating target assembly. The emerging gamma rays are allowed to fall on sandwiches of 30 mg/cm^2 thorium foils and 8 μm Kimfol films which serve as track recorders of the photofission fragments. The sandwiches are placed on a cylindrical surface coaxial with the proton beam. The energy of the gamma rays varies with the angle θ relative to the beam

as a result of the Doppler shift. The average energy dispersion is $\sim$ 200 eV/degree. An efficiency calibrated Ge(Li) detector (not shown) located at $\theta = 90^{o}$ serves to determine the absolute intensity of the gamma rays.

The developed[7] Kimfol films are scanned for fission tracks by a vidicon camera[8] which determines the positions of the tracks.

The photofission cross section is shown in Fig. 1 versus the gamma-ray energy. To compute the cross section, the efficiency of the Kimfol film[7] for counting fission fragments as a function of the depth in the foil from which the fragments emerge and the angle at which they enter the film was determined. The efficiency was folded with the angular distribution[9] of the fragments.

Resonances, in ^{29}Si, ^{42}Ca, ^{34}S and ^{25}Mg, yielding gamma rays of 6180, 6172, 6140, 6073 and 5871 keV at 90^{o} to the proton beam were used. The proton energies were well below the (p,n) thresholds of all targets. The intensity of photons from undesired branching did not exceed 10% in any of the cases. To match the spectra taken at the average photon energies of 6180 and 6172 keV it was important to measure accurately the energy difference between these two lines. This was found to be 7.7 ± 0.5 keV. The uncertainties in the magnitude of the cross section at the matching point do not exceed 15%. Unfortunately, with the present setup it was impossible to obtain an overlap of the two spectra. The instrumental gamma ray energy uncertainty was $\sim$ 200 eV in the runs with ^{42}Ca and ^{34}S targets and < 500 eV in the remaining two runs. The natural width of the ^{29}Si resonance is[10] 179 ± 5 eV. The widths of the other resonances are unknown but an upper limit of 1 keV can be obtained from their excitation curves. From the observed structure in Fig. 1 the overall photon energy resolution is seen to be better than 500 eV.

The average values of the cross sections over the photon energy range for each proton resonance are in good agreement with the results of Dickey and Axel [4] and Caldwell et al.[11] They are somewhat higher than those of Knowles et al. [5]

Well established peaks appear in all spectra. The probability that these peaks represent resonances in the photon absorption cross section is negligible given the fact that this would require for each resonance a ground-state radiative transition width $\sim$50 times larger than the average. It should also be noted that no structure has been found at higher excitation energies.[6] We therefore assume that the underlying states are compound levels of spin and parity 1^- in the second well of the barrier.

The average spacing of the nine peaks at 6.16 MeV is 1.6 ± 0.4 keV. From the constant temperature level-density formula with parameters given by Bjornholm and Lynn[1] we find the energy of the second minimum $E_{II}=2.8 \pm 0.1$ MeV, in good agreement with previous determinations [4,12]

The average widths W of the observed resonances at each excitation energy can be computed from the energy dependence of the fission probability.[13] The results listed in Table I are consistent with the experimental widths within the limits determined by the photon energy resolution.

The average area of a class II compound resonance at an excitation energy below the neutron separation energy can be written in the form[1]

$$A = \sigma_\gamma \pi^{\frac{1}{2}} D_I \Gamma_{IIf} \Gamma_{IIc} (\pi \Gamma_{II}^2 \Gamma_\gamma^2 + 2 D_I \Gamma_{IIc} \Gamma_{IIf} \Gamma_\gamma)^{-\frac{1}{2}} S,$$

where σ_γ is the average gamma ray absorption cross section, D_I is the average level spacing of class I compound states, Γ_{IIc}, and Γ_{IIf} are the coupling width and fission width of class II compound states respectively; $\Gamma_{II} = \Gamma_{IIc} + \Gamma_{IIf}$, Γ_γ is the average total gamma decay width of class I compound states, and S is the width fluctuation factor.

If there are several fission channels of a given spin and parity J^{π} differing in the spin projection on the fission axis K and having incompletely damped vibrational resonances in the second well at excitation energies $E_{IIv}^{(K)}$, the widths Γ_{IIc} and Γ_{IIf} are[13]

$$\Gamma_{IIc,f} = (D_{II}/2\pi) \sum_K \Gamma_{A,B}^{(K)} \Gamma_w ((E-E_{IIv}^{(K)})^2 + (\Gamma_{IIv}^{(K)}/2)^2)^{-1},$$

where D_{II} is the class II compound level spacing, $\Gamma_{A,B}^{(K)} = T_{A,B}^{(K)} \hbar\omega_{II}^{(K)}/2\pi$, $\hbar\omega_{II}^{(K)}$ is the level spacing of the vibrational states, Γ_w and $\Gamma_{IIv}^{(K)}$ are their damping and total widths respectively, $T_A^{(K)}$ and $T_B^{(K)}$ are the penetrabilities for channel K of barriers A and B respectively.

If the barrier for channel K has a third well with a vibrational resonance at $E_{IIIv}^{(K)}$, then $T_B^{(K)}$ in the expressions above has to be replaced by

$$T_{BC}^{(K)} = \Gamma_{IIIB}^{(K)} \Gamma_{IIIC}^{(K)} ((E-E_{IIIv}^{(K)})^2 + (\Gamma_{IIIv}^{(K)}/2)^2)^{-1},$$

where $\Gamma_{IIIB,C}^{(K)} = T_{B,C}^{(K)} \hbar\omega_{III}^{(K)}/2\pi$, and $\Gamma_{IIIv}^{(K)}$ and $\hbar\omega_{III}^{(K)}$ are the width of the resonance, and the level spacing of the vibrational states in the third well respectively.

For parabolic barriers $T_i^{(K)} = (1 + \exp(2\pi(E_i^{(K)}-E)/\hbar\omega_i^{(K)}))^{-1}$ where $E_i^{(K)}$ and $\hbar\omega_i^{(K)}$ are the heights and curvatures of the first (i = A) second (i = B) and third (i = C) barriers for channel K.

The average areas of the observed resonances at the four excitation energies are compared in Table I with the values calculated for a double-humped and a triple-humped barrier. The calculations were done with the barrier parameters listed in Table II and[4] σ_γ = 25 mb and Γ_γ = 31 meV at 6 MeV.

The information on the gross structure in the fission cross section, which is necessary for the area calculations, is somewhat uncertain. A

broad resonance at 6 MeV has been well established.[4,5] In addition, Knowles et al.[5] reported resonances at 5.92 and 6.11 MeV, each ~ 50 keV wide. These resonances cannot be clearly discerned in the spectra of Dickey and Axel[4] and those of Janszen et al[15]; the latter's obtained with an energy resolution of 17 keV. Therefore, in the calculations with the double-humped barrier we assumed a single resonance with a damping width of 0.2 MeV.

The results are in agreement with the experimental values when the areas at 6.14 and 6.17 MeV are averaged together and represented by a single value at 6.16 MeV, reflecting the possibility that the difference between the observed areas at the two energies could be due to width fluctuations.

The barrier parameters listed in Table II are close to the values obtained by fitting the measured[4,7] photofission cross sections between 5.5 and 11.5 MeV. It should be noted however that fits to average cross sections do not, in general, allow a unique determination of barrier parameters. The present results provide direct evidence for an inner barrier substantially higher than the one predicted by Möller and Nix. (The uncertainties in the 0^- barrier heights are $\pm$ 0.2 MeV). They also provide a unique determination of the depth of the second well.

In the calculations with the triple-humped barrier the narrow resonances reported by Knowles et al. were taken into account and assumed to correspond to vibrational states in the third well. To obtain a better fit to our data we increased the energy of the higher resonance to 6.12 MeV. The broad 6 MeV resonance was assumed to be located as before in the second well.

Agreement with the measured areas is somewhat better than in the case of the double-humped barrier. The increase in the resonance areas at 6.14 MeV can be understood as resulting from enhancement of the fission widths of the class II compound states owing to their coupling to the 6.12 MeV resonance.

However, because of the limited extent of the present data and large errors of the measured areas, it is impossible to conclude with certainty whether the observed increase confirms the 6.12 MeV resonance and, consequently, whether a third well exists in the fission barrier of ^{232}Th. More extensive measurements at subbarrier energies, using properly chosen (p,γ) resonances, are necessary to reach such a conclusion.

The authors wish to thank P. Punyasena for help in the processing of the kimfol films. Thanks are due to D. King and W. Stuber for their assistance in obtaining the high proton beam currents. This work was supported in part by the USDOE and by the PSC-BHE Faculty Research Award Program of CUNY.

References

1. S. Bjornholm and J.E. Lynn, Rev. Mod. Phys. 52, 725 (1980).
2. P. Moller and J.R. Nix, Proc. Third Int. Symp. Phys. and Chem. of Fission, Rochester 1973 (IAEA, Vienna 1974) Vol. 1, p. 103.
3. J. Blons, C. Mazur, D. Paya, M. Ribrag and H. Weigmann, Phys. Rev. Lett. 41, 1282 (1978).
4. P.A. Dickey and P. Axel, Phys. Rev. Lett. 35, 501 (1975).
5. J.W. Knowles, W.F. Mills, R.N. King, B.O. Pich, S. Yen, R. Sobie, L. Watt, T.E. Drake, L.S. Cardman and R.L. Gulbranson, Phys. Lett. 116B, 315 (1982).
6. T.R. Yeh and H. Lancman, IEEE Trans. Nucl. Sci. NS-28, 1289 (1981).
7. T.R. Yeh and H. Lancman, Nucl. Instr. Meth. 179, 141 (1981).
8. H.X. Zhang, T.R. Yeh and H. Lancman, Nucl. Instr. Meth. 214, 391, 1983.
9. N.S. Rabotnov, G.N. Smirenkin, A.S. Soldatov, L.N. Usachev, S.P. Kapitza and Yu. M. Tsipenyuk, Yad. Fix. 11, 508 (1970) Sov. J. Nucl. Phys. 11, 285 (1970) .
10. P.M. Endt and C. Van der Leun, Nucl. Phys. 214, 246 (1973).
11. J.T. Caldwell, E.J. Dowdy, B.L. Berman, R.A. Alvarez and P. Meyer, Phys. Rev. C21, 1215 (1980).
12. B. Back, O. Hansen, H.C. Britt and J.D. Garett, Phys. Rev. C9, 1924 (1974).
13. P. Glassel, H. Rosler and H.J. Specht, Nucl. Phys. A256, 220 (1976).
14. H.X. Zhang, T.R. Yeh and H. Lancman, Proc. Int. Conf. Nucl. Phys. 1, D121, Florence, Italy, 1983.
15. H. Janszen, S. Brandenburg, R. DeLeo, M.N. Harakeh, B. Visscher and A. van der Woude, Proceedings, Conf. Dynamics of Nucl. Fis. and Related Coll. Phenom. Bad Honnef, Germany, (Springer Verlag, 1981), p. 95.

TABLE I

AVERAGE AREAS AND WIDTHS OF RESONANCES

E (MeV)	A(b.eV)			W (eV)	
	Expt	Calc[a]	Calc[b]	Calc[a]	Calc[b]
6.17	5.1 ± 1.7	5.0	4.7	257	240
6.14	13.0 ± 4.0	5.7	11.0	304	493
6.07	3.1 ± 1.5	7.2	7.9	421	434
5.87	0.9 ± 0.4	1.3	1.2	95	97

[a]Double-humped barrier.
[b]Triple-humped barrier.

TABLE II

FISSION BARRIER PARAMETERS

K	Barrier Heights (MeV)				
	Double-Hump[a]		Triple-Hump[b]		
	E_A	E_B	E_A	E_B	E_C
0^-	6.15	6.55	6.15	6.55	6.9
1^-	6.55	6.85	6.55	6.95	7.5

[a] $\hbar\omega_A = \hbar\omega_{II} = 0.9$ MeV; $\hbar\omega_B = 0.65$ MeV for both K barriers.
These values supersede the slightly different ones reported earlier.[14]

[b] $\hbar\omega_A = \hbar\omega_{II} = 0.9$ MeV; $\hbar\omega_B = 1.4$ MeV; $\hbar\omega_{III} = 1.0$ MeV; $\hbar\omega_C = 1.2$ MeV for both K barriers.

Figure Caption

Photofission cross section of ^{232}Th. The vertical bars represent counting statistical errors only. The solid lines were obtained by Gaussian fitting. The inset in the right upper corner shows the geometrical setup of the experiment.

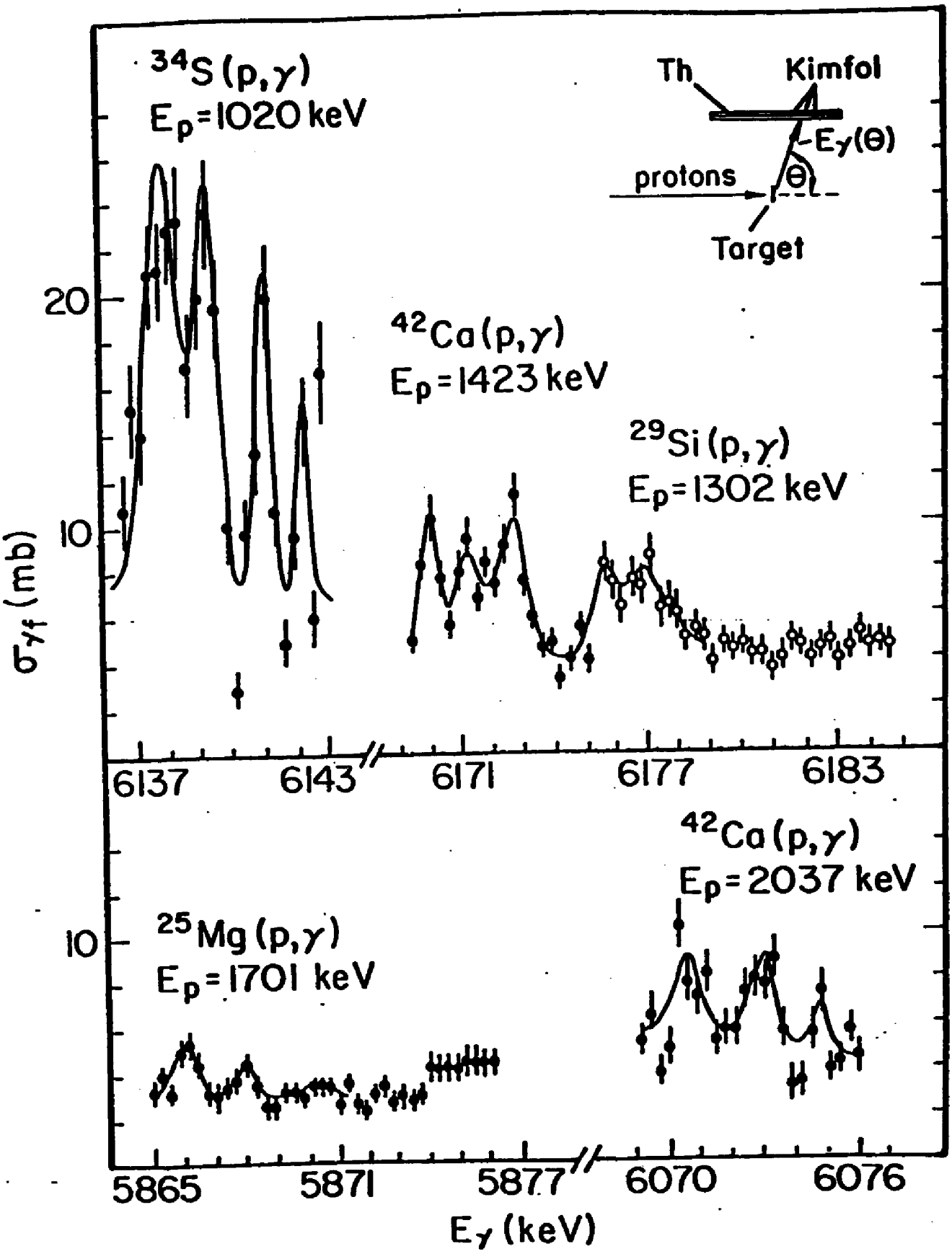
$^{34}S(p,\gamma)$
E_p=1020 keV
Th
Kimfol
$E_\gamma(\theta)$
protons
θ
Target
20
$^{42}Ca(p,\gamma)$
E_p=1423 keV
$^{29}Si(p,\gamma)$
E_p=1302 keV
10
$\sigma_{\gamma f}$ (mb)
6137
6143
6171
6177
6183
$^{42}Ca(p,\gamma)$
E_p=2037 keV
10
$^{25}Mg(p,\gamma)$
E_p=1701 keV
5865
5871
5877
6070
6076
E_γ (keV)

Fig. 1

The Photofission Cross Section of ^{232}Th

H.X. Zhang, T.R. Yeh* and H. Lancman
Physics Department
Brooklyn College of the City University of New York
Brooklyn, New York 11210

Abstract

The photofission cross section of ^{232}Th was measured in the energy range 5.8 - 12 MeV with an average photon energy resolution $\approx$ 600 eV. Intermediate structure was observed at 5.97 and 6.31 MeV. The experimental fission probability and various properties of the intermediate structure were found to agree with calculated values based on a double-humped fission barrier. The features of this barrier, a rather high first hump and a deep secondary well, are quite different from those predicted by current theoretical barrier calculations.

Nuclear Reactions ^{232}Th (γ,f), E = 5.8 - 12 MeV, measured σ (γ,f), deduced fission probability, class II compound levels, fission barrier parameters.

PACS number 25.85. Jg

1. Introduction

Since the discovery of the double-humped fission barrier in actinide nuclei extensive experimental and theoretical work has been done on various aspects of fission.[1] Of great value have been experimental investigations at excitation energies in the vicinity of the barrier because of the information they supply on the details of its character and shape. Very fruitful in this respect have been experiments on particle transfer reactions leading to fission[2,3] as well as experimental studies of neutron induced fission.[1] The latter in particular, because of their characteristically high neutron energy resolution, proved to be an excellent tool for investigating the complex level structure at subbarrier excitation energies. As a result of these efforts the main features of the fission barrier are now well understood.

Persisting interest in the fission of thorium isotopes has been caused in part by the difficulty in resolving the question of the existence of a theoretically predicted third minimum in their fission barriers.[1,4] The most direct evidence in favor of such a complex barrier has been provided by the observation[5] of rather narrow resonances in neutron induced fission of ^{231}Th and ^{233}Th. Fine structure observed within these resonances in high resolution measurements has been interpreted as corresponding to rotational bands built on undamped vibrational states. Various features of this structure, combined with data on cross sections at excitation energies above the fission barrier,[1] appear to be in support of a triple humped barrier with an inner barrier A considerably lower than barriers B and C. However, it has been shown by Lynn[6] that the observed structure could also result from coupling of single particle and vibrational motion in these nuclei.

In ^{232}Th, whose barrier is also expected[4,7,8] to be triple-humped, subbarrier excitation energies are not accessible in neutron induced fission because the neutron separation energy is higher than the barrier, but such energies can be reached in photofission. Accurate photofission measurements are best done with monochromatic gamma rays of variable energy. Such measurements have been done on ^{232}Th at $E_\gamma < 8$ MeV by Dickey and Axel,[9] and by Knowles et al.[10] with tagged bremsstrahlung having an energy resolution of 70 keV and 13 keV, respectively. In both cases the photofission cross section exhibits structure, the most prominent manifestation of which is a broad resonance at 6 MeV. We have recently[11] reported results of measurements of the photofission cross section of ^{232}Th at excitation energies close to the top of the barrier. The necessary photons were derived from (p,γ) resonances in several light nuclei. They had an energy resolution better than 500 eV. These measurements revealed resonances resulting from compound states in the second well of the barrier (intermediate structure). Various properties of this structure could be understood within the framework of the double-humped barrier although the possibility of a shallow third minimum could not be excluded.

Although the details of the shape of the fission barrier are reflected most directly by the behavior of the fission cross section at excitation energies in the vicinity of the barrier, measurements at higher photon energies also provide useful information. Such measurements are also important for the understanding of the fission decay of the giant quadrupole resonance.[12,13] Existing data has been obtained using quasi monochromatic photons from annihilation of positrons in flight. The energy resolution

of such photons is ~ 250 keV. Cross sections obtained by Veyssiere et al.[14] for several actinide nuclei are in substantial disagreement with the more recent results of Caldwell et al.[15] In the case of ^{232}Th the results of the two experiments differ by about 30% on the average. Recently reported measurements by H. Ries et al[16] on ^{235}U and ^{238}U, involving counting of fission fragments instead of neutrons as in the two other experiments, appear to confirm the values reported by Veyssiere for these two nuclei. However, results of Arruda-Neto et al[13] are in better agreement with the data of Caldwell.

The aim of the present measurements was to continue the investigations of intermediate structure over a wider energy range than the one reported earlier[11], and to extend the cross section measurements to higher energies in order to resolve the existing discrepancy between the published values of the cross sections. Preliminary results of this work have been described before.[17]

2. Experimental Setup and Procedures

The (p,γ) resonances chosen for these experiments are characterized by small natural width, large gamma ray yield, and decay by emission of only, or predominantly, one gamma ray with an energy higher than 5 MeV. Since the lifetime of a typical resonance is considerably shorter than the average stopping time of the recoiling compound nucleus in the material of the target, the energy of the emitted gamma ray is fully Doppler shifted. It varies with the angle of emission θ relative to the proton beam (see Fig. 1) according to the expression $E_\gamma = E_o\ (1 + (v/c)\cos\theta)$, where

v is the velocity of the recoiling nucleus. A typical value of $dE_\gamma/d\theta$ is $\gtrsim 300$ eV/degrees at $\theta = 90°$, and a typical photon energy range is ~ 20 keV.

Since high proton beam currents, $\sim 150\,\mu$A on the average, have to be used in order to assure an adequate photon flux, a target chamber designed[18] to withstand the large beam power dissipation was employed. The target materials were deposited on a water cooled thin Ta foil. The foil, mounted at the end of a bellows, vibrated in two mutually perpendicular directions in the plane perpendicular to the proton beam, spreading the beam over a large target area. High vacuum was maintained in the chamber to prevent deposit of contaminations on the target. In choosing the target materials, care was taken to avoid isotopes with (p,n) thresholds below the proton energy for the particular (p,γ) resonance. Each Ta foil was thoroughly cleaned and repeatedly heated in vacuum before the target was deposited.

The experimental setup was the same as the one described before.[11,17] Foils of thorium, 30 mg/cm^2 thick, containing 99.9% of ^{232}Th were sandwiched between 8μm thick strips of polycarbonate film (Kimfol). The sandwiches were located on a cylindrical surface coaxial with the proton beam (Fig. 1) which was provided by the Brooklyn College Dynamitron accelerator. The Kimfol film served as the fission fragment track detector. In order to determine the gamma ray intensity and spectrum, a large, efficiency calibrated, Ge(Li) detector (not shown) was placed at 90° to the proton beam.

To make the handling of the sandwiches manageable, the thorium foil was cut into 5 cm x 5 cm squares. Each square was covered by a 100 μg/cm^2

layer of gold on both sides to protect its surfaces from oxidation. It was necessary to use 90 such squares to assure an adequate counting rate of the fission fragments.

The efficiency calibration of the Kimfol film for counting the thorium fission fragments, and the procedures used in developing the film were described elsewhere.[19] The scanning of the developed film for fission fragment tracks was done with a high-resolution vidicon camera. A detailed description of the setup used for scanning was also given elsewhere.[20]

3. Data Reduction

In the cylindrical geometry used here, fission fragments produced by photons of energies between E_γ and $E_\gamma + \Delta E_\gamma$ are created in strips of foil defined by the intersections of the cylindrically shaped foil with cones of vertex angles θ and $\theta + \Delta\theta$ originating at the proton target (see Fig. 1).

The photofission cross section $\sigma_{\gamma f}$ at photon energy E_γ is related to the fission fragment counts $N(E_\gamma)$ in a strip of width $m(\theta)$ corresponding to an energy interval ΔE_γ by the expression

$$N(E_\gamma) = \frac{2I(\theta)}{4\pi r^2(\theta)} \sigma_{\gamma f}(E_\gamma) n l m(\theta) f(\theta) . \qquad (1)$$

Here $I(\theta) = I\, W(\theta)\, R(\theta)$ is the intensity of the gamma rays at angle θ, I is the intensity of the photons coming from the proton target, $W(\theta)$ is the photon angular distribution function, and $R(\theta)$ accounts for absorption of the photons on their way to the strip, n is the number of target nuclei

per unit volume, L is the length of the strip, $r(\theta)$ is its distance from the photon source, and

$$\eta(\theta) = \iiint F(\beta)\Omega(1,\alpha)\sin\beta d\beta d\varphi dl \ , \qquad (2)$$

where $F(\beta)$ accounts for the angular distribution of the fission fragments[21] relative to the direction of the gamma rays, and $\Omega(1,\alpha)$ is the efficiency of the Kimfol film[19] for detecting fragments emitted from depth 1 in the foil at an angle α to the normal. The angles θ, α, β, and the azimuthal angle φ are related by

$$\cos\alpha = \cos\beta\sin\theta - \cos\theta\sin\beta\sin\varphi \ . \qquad (3)$$

The photofission cross section is found for each energy E_γ by adding the numbers of tracks counted in strips found at angle θ in all Kimfol films. In plotting the cross section versus the photon energy, the choice of the energy interval per channel ΔE_γ was dictated by the total number of accumulated counts at a given (p,γ) resonance and by the photon energy resolution.

4. Results and Discussion

A. The Photofission Cross Section

The photofission cross sections obtained with gamma rays from several (p,γ) resonances are shown in Fig. 2. The target isotope and proton resonance energy are indicated in each case. Twenty one such spectra were taken in the photon energy range from 5.8 to 12 MeV. The average duration of each run was $\sim$ 20 hours. The statistical accuracy of the counts, shown

by the error bars, varies from spectrum to spectrum, reflecting the fluctuation of the strength of the (p,γ) resonances.

The photon energy resolution depends on several factors. Among them are the angular photon energy dispersion, the accuracy of the alignment of the films relative to the proton beam, the accuracy of the determination of the track position,[20] and the natural width of the (p,γ) resonances. In cases where the last contribution is negligible, the energy resolution ranges from ~200 eV for the lower photon and resonance proton energies and heavier (p,γ) target isotopes to ~ 700 eV for the high photon and proton energies and light target isotopes.

The cross sections averaged over the photon energy range at each (p,γ) resonance are plotted versus the average photon energy in Fig. 3. Two adjacent spectra at 6.17 MeV are represented by one point. The error bars include counting errors (negligible), errors in the efficiency calibration of the gamma ray and fission fragment detectors, uncertainties in the angular distribution of the fission fragments and the gamma rays, and uncertainties in the alignment of the thorium foils and Kimfol films relative to the proton target. The plotted cross sections were corrected for contributions caused by the unwanted gamma rays emitted from some (p,γ) resonances. Except for one case, these corrections did not exceed 10% of the presented values. The sum of the contributions from fission caused by neutrons from (γ,n), $(\gamma,2n)$, and fission, as well as the contribution from (γ,nf), were estimated to be smaller than 2%.

Our results are in good agreement with those of Dickey and Axel,[9] and at energies above 9 MeV those of Caldwell et al.[15] They are systematically higher than the results of Knowles et al[10] (not shown). They are also higher than the cross sections reported by Veyssiere et al.[14] The general features of the cross section as a function of energy have been known for some time. The rapid decrease in the cross section starting at 6.45 MeV has been shown to be caused[23] by competition from the (γ,n) channel which opens at 6.43 MeV. The broad resonance at 6 MeV, clearly seen in Knowles' and Dickey's data, has been confirmed by (p, p'f) measurements.[22] It should be kept in mind while comparing the various data that our results are obtained by averaging over an energy interval at least an order of magnitude smaller than in the other experiments.

B. The Fission Probability

The fission probability is obtained by dividing the photofission cross section by the total gamma-ray absorption cross section σ_γ. It is shown in Fig. 4 versus the gamma ray energy. The values of σ_γ were taken directly from Ref. 15 for photon energies higher than 9 MeV. Below this energy they were obtained by extrapolation.[15] The calculated fission probability that provides the best fit to the data up to the $(\gamma,2n)$ threshold is shown by the solid line. It was computed using the program FISSAL developed for a double-humped fission barrier by Back and Britt.[24] The statistical model on which the program is based is discussed in detail by Back et al.[2] We therefore describe it here only briefly.

The fission probability is given in its usual form

$$P_f(E) = \sum_{J^\pi} \alpha(EJ^\pi) \frac{\Gamma_f(EJ^\pi)}{\Gamma_t(EJ^\pi)} S \ , \tag{4}$$

where $\alpha(EJ^\pi)$ is the probability of populating a state with spin J and parity π by photoabsorption, $\Gamma_t = \Gamma_f + \Gamma_n + \Gamma_\gamma$ is the total width of the state, and Γ_f, Γ_n and Γ_γ are its partial widths for decay by fission, neutron emission and gamma-ray emission, respectively. S is a correction factor for width fluctuation.[1] All widths are averaged over many states at excitation energy E . The averaging is expected to obliterate structure resulting from compound states in both wells while preserving the much wider spaced vibrational resonances in the second well.

The gamma-ray decay width is calculated by summing over all transitions to states at lower energy in the first well assuming that only E1 transitions take place. Similarly, the neutron emission width is computed by summing the transmission coefficients for transitions to all possible final states in the A-1 nucleus.

The average fission width is obtained from

$$\Gamma_f(EJ^\pi) = \frac{D_I(EJ^\pi)}{2\pi} \sum_K T_f^K(EJ^\pi) \ , \tag{5}$$

where D_I is the average level spacing at ground state deformation, and T_f^K are the barrier penetrabilities for the transition states with different spin projections K on the nuclear symmetry axis. These penetrabilities are found analytically by solving the Schrödinger

equation for a double humped fission barrier. The barrier is formed by joining smoothly three parabolic sections which represent its two humps and the well between them (second well). The parameters that characterize the barrier are the heights of the first and second humps E_A and E_B, their curvatures $\hbar\omega_A$ and $\hbar\omega_B$, the minimum of the second well E_{II}, and its curvature $\hbar\omega_{II}$. The penetrability found in this way exhibits resonances at energies of vibrational states in the second well. To account for the damping of these states into the compound states in the second well, an imaginary term is added to the potential. This term is a parabolic function of deformation centered at the deformation of the second well. Its minimum value is

$$-W(E) = -w(E - E_{II} - \Delta_n - \Delta_p) - W_o \,, \tag{6}$$

where Δ_n and Δ_p are the neutron and proton pairing gaps. As a result of the addition of the imaginary term to the potential, the penetrability T_f becomes a sum of two parts

$$T_f = T_D + T_I, \tag{7}$$

where T_D represents direct and T_I indirect fission i.e. fission preceeded by the excitation of compound states in the second well.

When several transition states contribute to the process, the sum in Eq. 5 has to be replaced by $(N_D + N_I)$, where $N_D = \sum_K T_D^K$, and, under the assumption of K mixing in the second well, $N_I = N_{abs} N_B/(N_A+N_B)$. Here $N_{abs} = \sum_K A^K$, and $N_{A,B} = \sum_K T_{A,B}^K$, where A^K is the flux absorbed in the second well from transition state K, and $T_{A,B}^K = (1 + \exp[2\pi(E_{A,B}^K - E)/\hbar\omega_{A,B}^K])^{-1}$ are the Hill-Wheeler penetrabilities of barriers A and B for transition states K.

In the absence of damping, all $A^K = 0$, whereas for complete damping, all $T_D^K = 0$. The latter case is assumed in the nonresonance version of the program which is used to calculate the fission probability at energies well above the barrier. In this case the probability is decided by the density of states at barriers A and B. This density, in turn, strongly depends on the symmetry of the fissioning nucleus at the deformation of each barrier. In the present calculation, following Back et al[2], we used the resonance version of the program at energies below 7.5 MeV; above that energy, the non-resonance version was used. However, we found that between 6.5 and 7.5 MeV the results obtained with the two versions differ insignificantly. Barrier A was taken to have axial asymmetry, reflection symmetry; barrier B axial symmetry, reflection asymmetry. The population probabilities for the states reached by electric dipole and quadrapole excitations were taken to be 0.98 and 0.02, respectively,[23] independent of excitation energy.

All barrier parameters cannot be uniquely determined by fitting the experimental fission probability. Fortunately, some can be found independently from other data. The value of E_{II} is determined by the density of class II states[11] at 6.16 MeV. The spacing of the resonances at 6.313 MeV, $D_{II} = 1.3 \pm 0.3$ keV, is in excellent agreement with this value. The average areas of the observed intermediate structure set the values of $E_A^{0^-}$ and $E_B^{0^-}$ at 6.15 ± 0.2 MeV and 6.55 ± 0.2 MeV, respectively.

The other parameters were varied to provide the best fit (solid line in Fig. 4). The results are compared with other determinations in Table I.

Although the overall agreement between the values of the parameters determined in different experiments is good, there are several exceptions. The values $E_A^{0^-}$ found by Van der Plicht et al[25] is too high to account for the measured average areas of the class II resonances. Our data confirm their value of $E_B^{0^+}$, which is higher than the values obtained in the other experiments. Our value for $E_B^{1^-}$ is somewhat higher than the two other values, however, of these two, the value from Ref. 11 was obtained by fitting the average areas of the class II resonances, which is not very sensitive to $E_B^{1^-}$. In the present case, $E_B^{1^-}$ is determined mainly by the fission probability at ~ 7 MeV, where the contributions of $K^\pi = 1^-$ and 0^- fission become comparable. The $J^\pi = 2^+$ barrier parameters cannot be determined from the present data because of the small value of $\alpha(2^+)$.

Given the theoretical prediction[4,7,8] of a rather low barrier A and a barrier B split by a third well, it is tempting to compare the calculated fission probability for such a barrier with the experimental data. If the first barrier is low, then, in order to account for the intermediate structure and the broad vibrational resonance, it is necessary to assume that the third well has a minimum at ~ 3 MeV. Since the low first barrier does not affect the fission probability at energies $\sim$ 6 MeV, the part of the barrier which has to be considered is the double humped part comprised of barriers B and C at higher deformations. To compute the fission probability we assume that both barriers B and C are axially

symmetric and reflection asymmetric,[8] and that they are characterized by parameters listed in Table I. The result is shown by the dashed line in Fig. 4. Agreement with experiment at higher energies can be improved by lowering $E_B^{0^+}$ by 200 keV, which results in the dotted line. Clearly, on the basis of the present data it is impossible to choose between this barrier and the ordinary double-humped one.

C. Intermediate Structure

a. Background

The spectra in Fig. 2 at 5974 and 6313 keV exhibit structure which we interpret as representing class II compound states in the second well of the barrier. As in the cases reported previously,[11] the observed peaks are superimposed on a rather high background. Its magnitude is determined by fitting each spectrum with a function

$$\sigma_b(E_\gamma) = a E_\gamma^2 + b E_\gamma + c, \quad \text{and } E_1 \text{ are the energies of the} \tag{8}$$

where $\sigma_b(E_\gamma) = a E_\gamma^2 + b E_\gamma + c$, and E_1 are the energies of the peaks. To compare the magnitudes of σ_b with theoretical expectations,

peaks. To compare the magnitudes of σ_b with theoretical expectations,

it is useful to express the cross section in terms of the fission probability. Thus $\sigma_{\gamma f}(E) = P_f(E)\ \sigma_\gamma(E)$, where it is assumed that the excitation energy $E = E_\gamma$.

Employing the picket-fence model for the class II states we can write for the fission probability at energy $E = E_1 + x$ below the (γ,n) threshold.

$$P_f(x) = \sum_{J\pi} \alpha \frac{\Gamma_f(x) + \Gamma_D}{\Gamma_f(x) + \Gamma_D + \Gamma_\gamma} S \quad . \tag{9}$$

We will assume that $\alpha(1^-)=1.0$.

When overlap of class II resonance tails is not neglected, $\Gamma_f(x)$ represents the sum of contributions from all class II states to the fission width at x. This has the form[2]

$$\Gamma_f(x) = \frac{\Gamma_{IIc}\Gamma_{IIf}D_I}{\Gamma_{II}D_{II}} \cdot \frac{\sinh(2\pi\Gamma_{II}/D_{II})}{\cosh(2\pi\Gamma_{II}/D_{II}) - \cos(4\pi x/D_{II})} , \qquad (10)$$

where Γ_{IIc}, Γ_{IIf} and Γ_{II} are, respectively, the coupling, fission, and total widths of the class II states. In the presence of several transition states K with incompletely damped vibrational resonances in the second well at energies E^K_{IIv}

$$\Gamma_{IIc,f} = \frac{D_{II}}{2\pi}\sum_K \Gamma^K_{A,B}\Gamma^K_w/((E - E^K_{IIv})^2 + (\Gamma^K_{IIv}/2)^2) , \qquad (11)$$

where

$$\Gamma^K_{A,B} = \frac{\hbar\omega^K_{II}}{2\pi} T^K_{A,B}) \qquad (12)$$

and Γ^K_w and Γ^K_{IIv} are, respectively, the damping, and total widths of the vibrational resonances. When damping in the second well is complete

$$\Gamma_{IIc,f} = \frac{D_{II}}{2\pi}\sum_K T^K_{A,B} .$$

The direct fission width Γ_D can be written in the form

$$\Gamma_D = \frac{D_I}{2\pi}\sum_K T^K_A T^K_B \left(1/2\pi + \frac{(\hbar\omega^K_{II}/2\pi)^2}{(E - E^K_{IIv})^2 + (\Gamma^K_{IIv}/2)^2}\right) . \qquad (13)$$

The first term in Eq. (13) arises from the coupling of the vibrational and compound states in the first well of the barrier. The often-omitted[3,26] factor $1/2\pi$ in this term was found by Bjørnholm and Lynn[1] to be necessary in order to account better for the ratio of the class I to class II squared vibrational wave functions, which enters into the calculation of Γ_D. The second term represents

enhancement of the direct fission width due to class II vibrational resonances. It can be obtained from the expression for the "resonant direct" fission width of Goldstone and Paul[26] by replacing their squared coupling matrix element V^2 with $D_I \hbar\omega_{II}/4\pi^2$. This replacement is consistent with Eq. (12) and is equivalent in our case to a value for the matrix element V = 0.3 keV, which is considerably lower than the value V = 3 keV determined by Goldstone et al[27] for several actinide nuclei. The smaller magnitude of V is consistent, within the doorway-state model,[26] with the experimental width(200 keV) of the vibrational resonance at 6.01 MeV, whereas the larger one yields a value of ~2 MeV for this width.

The fission probability $P_f(x)$ computed with the barrier parameters of Table I is plotted for two excitation energies in Fig. 5. Only two peaks are shown at each energy. The fission probability between these peaks $P_b = P_f(\frac{D_{II}}{2})$ is taken to represent the background that would be observed experimentally in these spectra. The values of P_b computed at the energies where intermediate structure was resolved in the present and previously reported[11] experiments are compared in Fig. 6 with the values of $P_b^{exp} = \sigma_b / \sigma_\gamma$ averaged over the measured spectrum at each energy. Agreement is very good.

b. Average Resonance Area

The average area of the class II resonances that one may expect to observe directly in a spectrum is

$$A = \sigma_\gamma \int_0^{D_{II}} (P_f(x) - P_b)\,dx \,. \qquad (14)$$

This can be written in the form

$$A = \bar{\sigma}_\gamma D_{II}(P_2 - P_1)\Gamma_\gamma/(\Gamma_\gamma + \Gamma_D) \ , \qquad (15)$$

where

$$P_1 = \frac{S\Gamma_f(x=D_{II}/2)}{\Gamma_f(x=D_{II}/2)+\Gamma_D+\Gamma_\gamma} \ ,$$

and

$$P_2 = SG((G+\cosh(\pi\Gamma_{II}/D_{II}))^2-1)^{-\frac{1}{2}} \ ,$$

with

$$G = \frac{\Gamma_{IIc}\Gamma_{IIf}D_I}{\Gamma_{II}(\Gamma_\gamma+\Gamma_D)D_{II}} \sinh(\pi\Gamma_{II}/D_{II}) \ .$$

It can easily be verified that when $\Gamma_{II} \ll D_{II}$ and $\Gamma_D \ll \Gamma_\gamma$ the second term in Eq. (14) disappears and Eq. (15) assumes the form given for A in Ref. 11, where direct fission and overlap of class II states were neglected. It is also interesting to compare $P_f(x)$ averaged over the intermediate structure with $P_f(E)$ given by FISSAL. When this is done, the difference is found to be about 5% on the average, in the energy range 6.0 - 6.3 MeV. A greater difference is found below the vibrational resonance because FISSAL yields a slightly lower value for the energy of this resonance than the experimental value taken for computing $P_f(x)$. After this is accounted for by a simple shift in energy of $P_f(x)$ relative to P(E), the two fission probabilities are remarkably similar in magnitude.

The areas obtained from Eq. (15) are compared with the average experimental resonance areas in Table II. The data reported previously are included, with one exception, in this comparison. The omitted value at 5.87 MeV was obtained with a (p,γ) resonance, which, as we have learned recently,[28] has a natural width of 1.7 keV. Therefore, the

structure observed at this energy may have reflected the existence of only the strongest class II resonances. Considering the fact that the experimental average areas in Table II are based on a limited number of peaks in each spectrum, the agreement with the calculated values is very good.

From Fig. 5 and the calculated areas listed in Table II, it is clear that near the top of the barrier, as the excitation energy increases, intermediate structure may be expected to become increasingly difficult to observe.

5. Conclusions

We have measured the photofission cross section in 20 narrow energy intervals between 5.8 and 12 MeV with an average photon energy resolution of $\sim$ 600 eV. The investigation of the intermediate structure was extended to 6.3 MeV. From studies of the properties of this structure and dependence of the fission probability on the excitation energy, we have determined the fission barrier parameters on the assumption of a double-humped barrier shape. The data confirms our previous finding that in ^{232}Th a barrier of 6 MeV is followed by a deep intermediate well with a minimum at 2.8 MeV. This is contrary to the theoretical predictions[4,7,8] of a much lower first barrier followed by two shallow wells. Indications that the first barrier in the adjacent ^{233}Th is also considerably higher than the one predicted theoretically and that it is followed by a deep secondary well were found by Perez et al[29] in their measurements of the ^{232}Th (n, f) cross section.

The present data is not sufficient to determine whether a tertiary well exists in the fission barrier of ^{232}Th. For this more extensive measurements of structure at low energy have to be done.

We wish to thank D. King and B. Stuber for their expert maintenance of the Dynamitron during the course of these experiments. The contributions of Drs. P.X. Zhu and M. Ismail during their stay at this laboratory are gratefully acknowledged. This work was supported in part by the U.S. Department of Energy and by the Professional Staff Congress - Board of Higher Education Faculty Research Award Program of the City University of New York.

References

* Present address: Inst. Nucl. En. Res., P.O. Box 3, Taiwan, ROC.

1. S. Bjørnholm and J.E. Lynn, Rev. Mod. Phys. 52, 725 (1980).
2. B.B. Back O. Hansen, H.C. Britt, and J.D. Garrett, Phys. Rev. C9, 1924 (1974).
3. P. Glassel, H. Rosler, and H.J. Specht, Nucl. Phys. A256, 220 (1976).
4. P. Moller and J.R. Nix, Proceedings of the Third International Symposium on the Physics and Chemistry of Fission, Rochester 1973 (International Atomic Energy Agency, Vienna, 1974) Vol. 1, p.103.
5. J. Blons, C. Mazur, D. Paya, M. Ribrag, and H. Weigmann, Nucl. Phys. A414, 1 (1984).
6. J.E. Lynn, J. Phys. G: Nucl. Phys. 9, 665 (1983).
7. J. Dudek, W. Nazarewicz, and A. Faessler, Nucl. Phys. A412, 61 (1984).
8. W.M. Howard and P. Moller, Atomic Data and Nucl. Data Tables 25, 219 (1980).
9. A. Dickey and P. Axel, Phys. Rev. Lett. 35, 501 (1975).
10. J.W. Knowles, W.F. Mills, R.N. King, B.O. Pich, S. Yen, R. Sobie, L. Watt, T.E. Drake, L.S. Cardman, and R.L. Gulbranson, Phys. Lett. 116B, 315 (1982).
11. H.X. Zhang, T.R. Yeh, and H. Lancman, Phys. Rev. Lett. 53, 34 (1984).
12. H. Stroher, R.D. Fischer, J. Drexler, K. Huber, U. Kneissl, R. Ratzek, H. Ries, and W. Wilke, and H.J. Maier, Phys. Rev. Lett. 47, 318 (1981).
13. J.D.T. Arruda-Neto, W. Rigolon, S.B. Herdade, and H.L. Riette, Phys. Rev. C29, 2399 (1984).
14. A. Veyssiere, H. Beil, R. Bergere, P. Carlos, A. Lepretre, and K. Kernbath, Nucl. Phys. A 199, 45 (1973).
15. J.T. Cadwell, E.J. Dowdy, B.L. Berman, R.A. Alvarez, and P. Meyer, Phys. Rev. C21, 1215 (1980).
16. H. Ries, G. Mank, J. Drexler, R. Heil, K. Huber, U. Kneissl, R. Ratzek, H. Stroher, T. Weber, and W. Wilke, Phys. Rev. C29, 2346 (1984).
17. T.R. Yeh and H. Lancman, IEEE Trans. Nucl. Sci. NS-28, 1289 (1981).

18. H.X. Zhang and H. Lancman, Nucl. Instr. Meth., A239, 459 (1985).

19. T.R. Yeh and H. Lancman, Nucl. Intr. Meth. 179, 141 (1981).

20. H.X. Zhang, T.R. Yeh,and H. Lancman, Nucl. Instrum. Methods 214, 391 (1983).

21. N.S. Rabotnov, G.N. Smirenkin, A.S. Soldatov, L.N. Usachev, S.P. Kapitza, and Yu. M. Tsipenyuk, Soviet Journal of Nucl. Phys. 11, 285 (1970).

22. H. Janszen, S. Brandenburg, R. De Leo, M.N. Harakeh, B. Visscher,and A. Van der Woude, Dynamics of Nuclear Fission and Related Collective Phenomena (Springer Verlag, Berlin, 1981) p. 95.

23. J.R. Huizenga and H.C. Britt, Proc. Int. Conf. Photonucl. Reactions and Applic. Asilomar 1973, edited by B.L. Berman (U.S. Atom. En. Comm. Office of Inform. Services,Oak Ridge,Tenn.1973) Vol. 2 p.833.

24. We wish to thank Dr. B. Back for providing us with a copy of the program.

25. J. Van Der Plicht, M.N. Harakeh, . A.Van der Woude,P.David,J.Debrus, H.Janszen,and J.Schulze,Nucl.Phys. A369,51 (1981).

26. P. Goldstone and P.Paul, Phys. Rev. C18, 1733 (1978).

27. P.D. Goldstone, F. Hopkins, R.E. Malmin,and P. Paul, Phys. Rev. C18, 1706 (1978).

28. G. Adams, E.G. Bilpuch, G.E. Mitchell, R.O. Nelson,and C.R. Westerfeldt, J. Phys. G: Nucl. Phys. 10, 1747 (1984).

29. R.B. Perez, G. de Saussure, J.H. Todd, T.J. Yang,and G.F. Auchampaugh, Phys. Rev. C28, 1635 (1983).

Figure Captions

Fig. 1. Part of the experimental setup showing a fission fragment emitted from depth 1 in the thorium foil. The sandwiches of Kimfol film and thorium foil are located on a cylindrical surface coaxial with the proton beam.

Fig. 2. Photofission cross section of ^{232}Th for several photon energies. The (p,γ) resonances used to produce the photons and the resonance proton energies are listed in each case. The photon energy resolution in the two spectra exhibiting structure was $\sim$ 300 eV.

Fig. 3. Photofission cross sections obtained in different experiments. The results of this work are averaged over the photon energy range at each (p,γ) resonance.

Fig. 4. Comparison of the fission probability of ^{232}Th with the results of calculations based on the statistical model. The solid line is for axially asymmetric, reflection symmetric barrier A and axially symmetric, reflection asymmetric barrier B. The dashed line is computed assuming axial symmetry, reflection asymmetry for both barriers. The dotted line is based on the same assumption as the dashed one but with $E_B^{0^+}$ lower by 200 keV.

Fig. 5. Intermediate structure in the fission probability calculated at two excitation energies.

Fig. 6. The background fission probability. The experimental points represent the average values of P_b^{exp}.

Table I. Fission barrier parameters of ^{232}Th (in MeV)

	K^{π}	Ref. 22	Ref. 1	Ref. 9	Ref. 25	Ref. 2	Ref. 11	This work
E_A	0^+	5.8	5.82	5.5	5.7	<5.5		5.82
	0^-	6.75		6.3	6.7		6.15	6.10
	1^-			6.5			6.55	6.55
$\hbar\omega_A$		0.9	1.0	0.9	0.9		0.9	1.0
E_B	0^+	6.75	6.22	6.1	6.6	6.15		6.40
	0^-	6.75		6.3	6.6		6.55	6.50
	1^-			6.9			6.85	7.25
$\hbar\omega_B$		1.2	0.75	0.5	1.2	0.5	0.65	0.7
E_{II}		3.0		3.0	3.0		2.8	2.8
$\hbar\omega_{II}$		1.5		1.5	1.5			0.9
W_o		0.05			0.05			0.05
w		0.25			0.15			0.15

Table II. Average areas and widths of resonances

E(MeV)	Area(b.eV)		Width(eV)
	Expt.	Calc.	Calc.
6.313	5.2±1.7	3.5	420
6.175	5.1±1.7	3.7	290
6.144	13.0±4.0	3.9	330
6.074	3.1±1.5	4.8	450
5.974	4.8±1.6	4.7	400

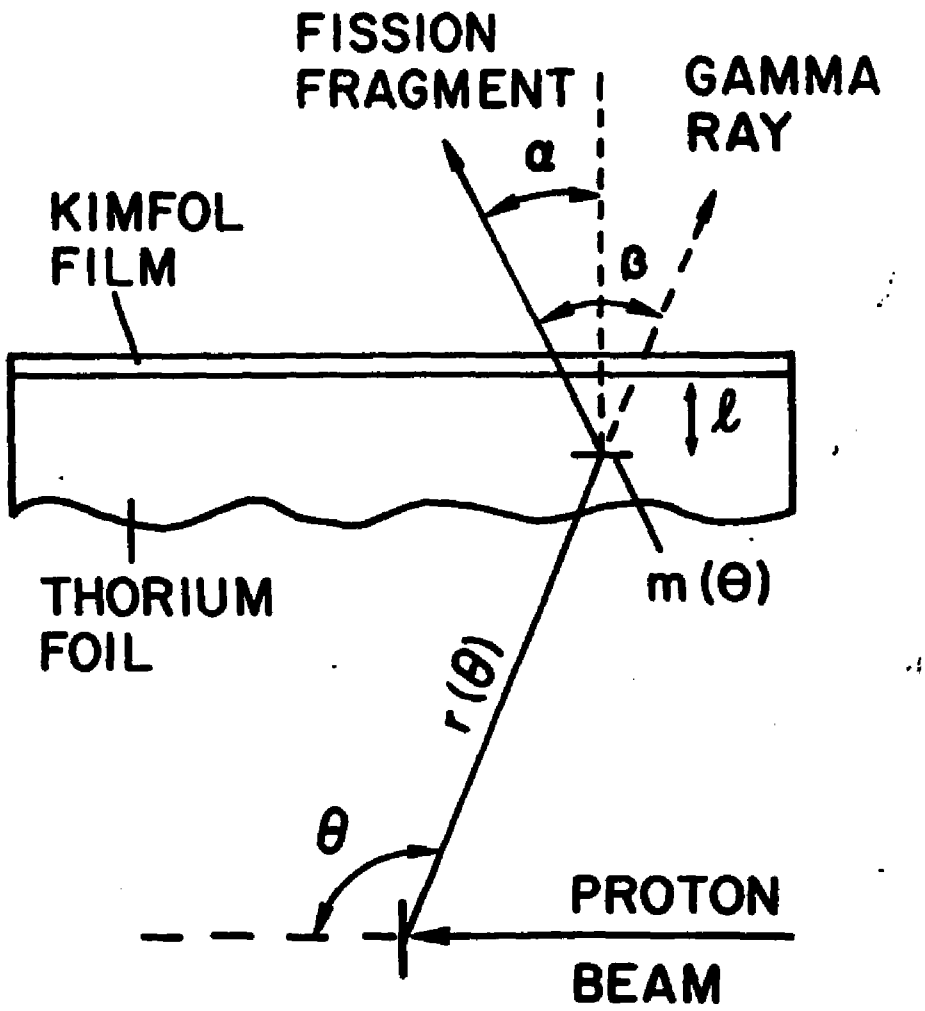
FISSION
FRAGMENT
GAMMA
RAY
α
β
KIMFOL
FILM
ℓ
THORIUM
FOIL
m (Θ)
r(Θ)
θ
PROTON
BEAM

Fig. 1

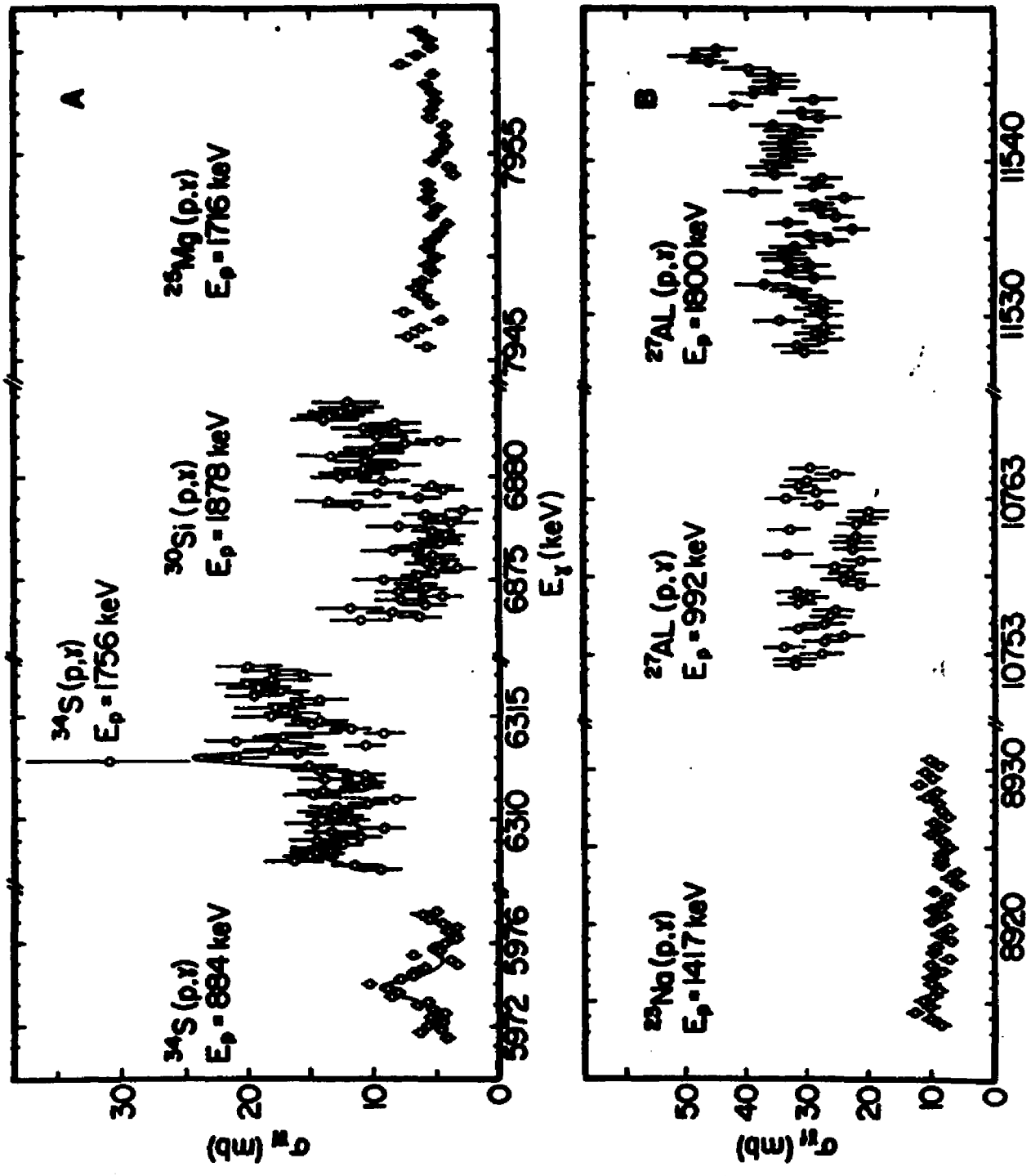
A
^{34}S(p,γ)
E$_p$ = 1756 keV
^{30}Si(p,γ)
E$_p$ = 1878 keV
^{26}Mg(p,γ)
E$_p$ = 1776 keV
^{34}S(p,γ)
E$_p$ = 884 keV
B
^{27}AL(p,γ)
E$_p$ = 1800 keV
^{27}AL(p,γ)
E$_p$ = 992 keV
^{23}Na(p,γ)
E$_p$ = 1417 keV
E$_γ$ (keV)
σ$_{tt}$ (mb)

Fig. 2

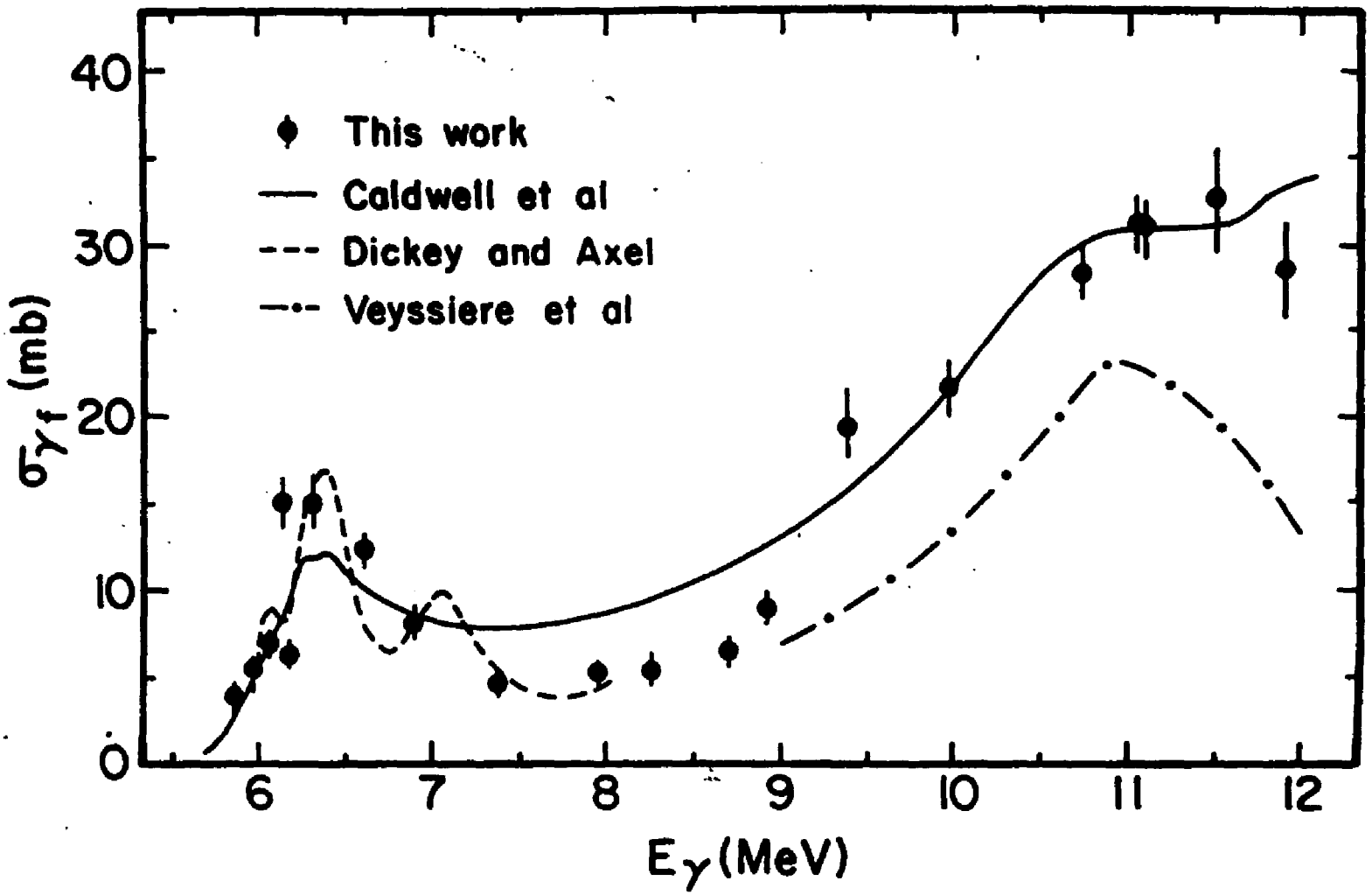
This work
Caldwell et al
Dickey and Axel
Veyssiere et al
$\sigma_{\gamma f}$ (mb)
E_γ (MeV)
0
10
20
30
40
6
7
8
9
10
11
12

Fig. 3

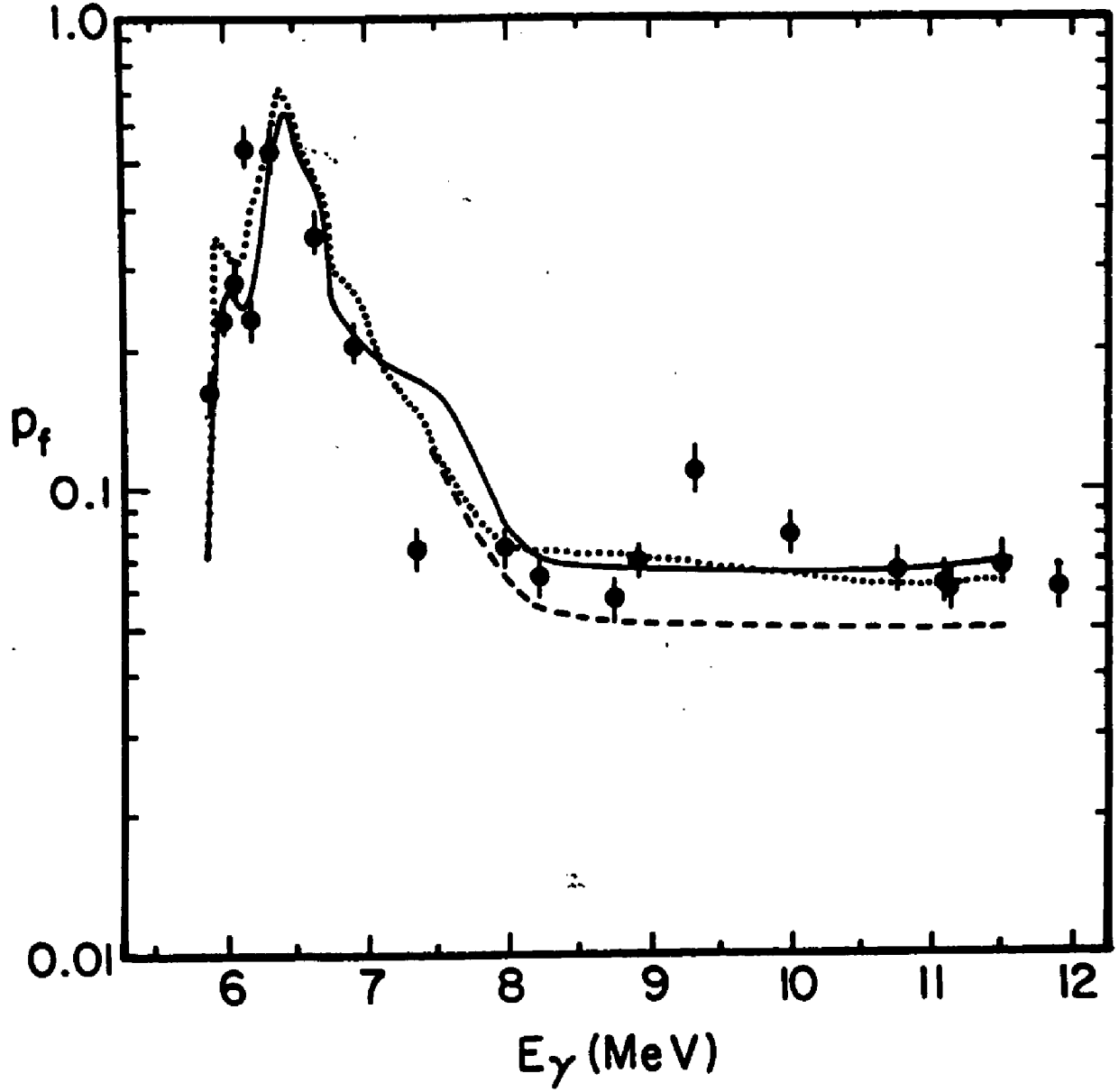

Fig. 4

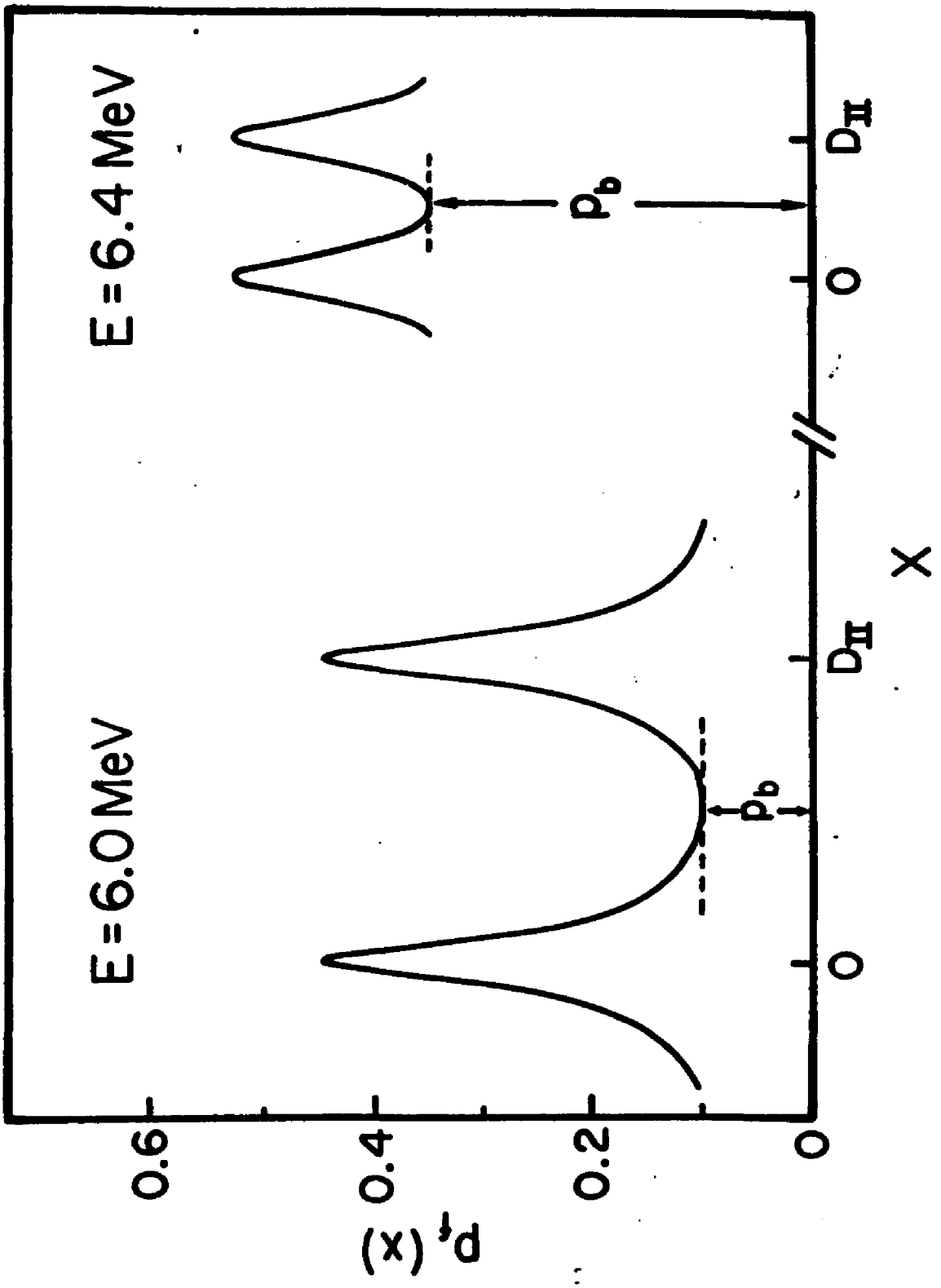

Fig. 5

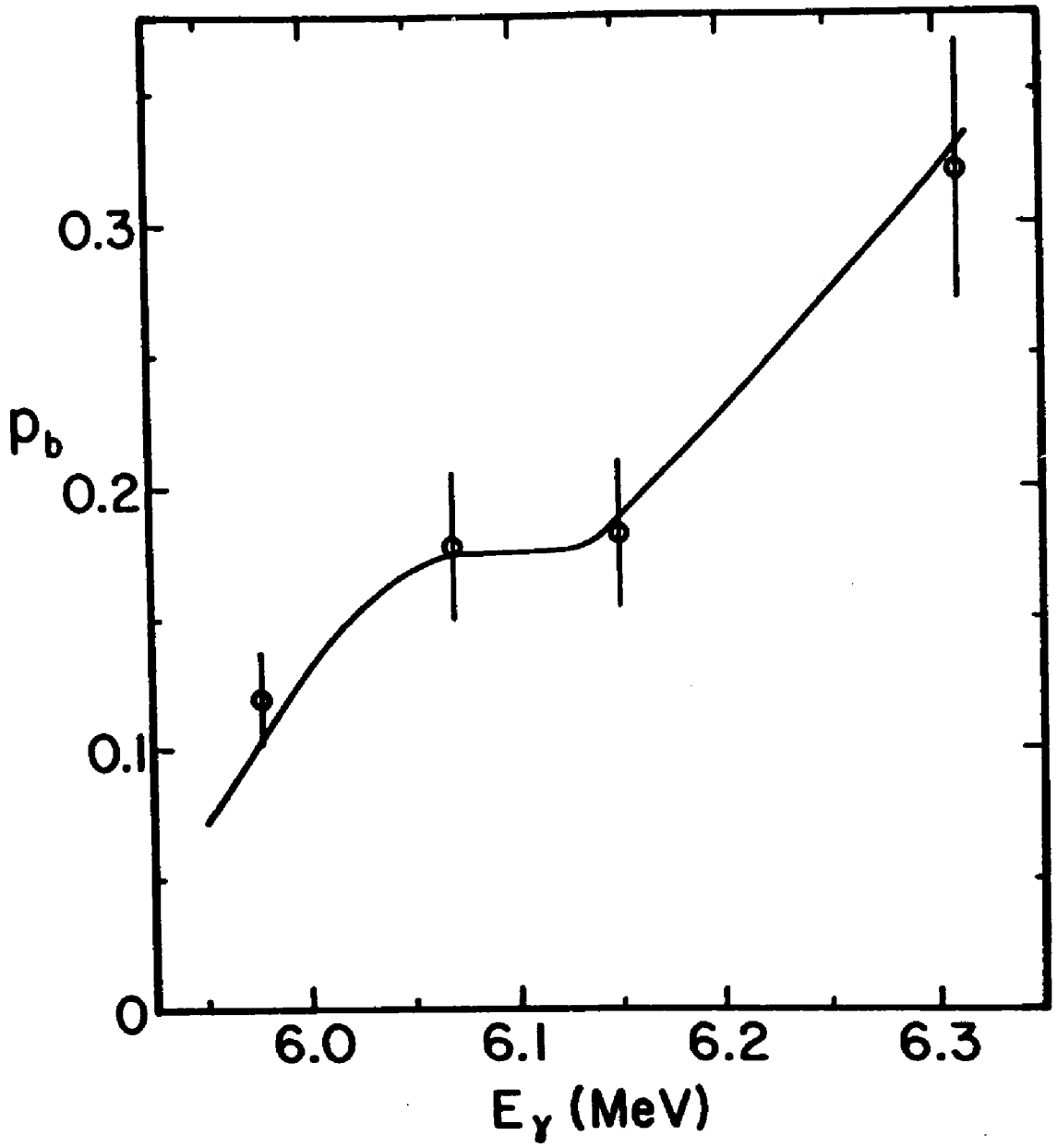

Fig. 6

APPENDIX I

Photofission cross sections of ^{238}U and ^{232}Th obtained with gamma rays from various (p,γ) resonances.

(p,γ) resonance			$\sigma_{\gamma f}$(mb)	
Target	E_p(keV)	E_γ (keV)	^{232}Th	^{238}U
^{25}Mg	1701	5871	3.9±0.5	8.2±0.8
^{34}S	848	5974	5.8±0.6	11.5±2
^{42}Ca	2037	6073	7.2±0.7	15.3±5
^{34}S	1020	6143	15.0±1.5	
^{42}Ca	1423	6172	7.2±0.6	5.9±0.6
^{29}Si	1302	6180	5.6±0.7	15.2±2
^{34}S	1756	6312	15.0±1.5	12.0±4
^{34}S	2073	6622	12.4±1.3	
^{30}Si	1878	6878	8.1±0.8	10.9±3
^{30}Si	1398	7377	4.6±0.4	10.4±1
^{25}Mg	1716	7954	5.3±0.5	12.4±1
^{30}Si	982	8244	5.5±0.5	16.5±1.6
^{30}Si	1480	8727	6.5±0.6	18.1±2
^{23}Na	1417	8923	9.8±1	24.0±2.5
^{27}Al	2488	9363	19.512	42.0±4
^{35}Cl	1519	9980	22.0±2	54.9±5
^{27}Al	992	10759	28.4±3	80.5±8
^{27}Al	1317	11072	31.5±3	96.1±9
^{27}Al	1381	11134	31.2±3	103.0±10
^{27}Al	1800	11537	32.8±3	80.6±8
^{27}Al	2203	11925	28.8±3	99.0±10
^{27}Al	774	12326		97.5±10

APPENDIX II

DERIVATION OF EQUATION (15) OF CHAPTER IV

The area of an observed peak in the photofission cross section is given by(see Fig.5 of Chapter IV)

$$A = \sigma_\gamma \int_0^{D_\Pi} (P_f(x) - P_b)\,dx, \qquad (1)$$

with

$$P_f(x) = \frac{\Gamma_f(x) + \Gamma_D}{\Gamma_f(x) + \Gamma_D + \Gamma_\gamma}, \qquad (2)$$

and

$$P_b = P_f\left(x = \frac{D_\Pi}{2}\right). \qquad (3)$$

It can be shown by means of simple algebraic manipulations that

$$P_f(x) - P_b = \frac{\Gamma_\gamma}{(\Gamma_\gamma + \Gamma_D)}\left(\frac{\Gamma_f(x)}{\Gamma_f(x) + \Gamma_D + \Gamma_\gamma} - \frac{\Gamma_f\left(\frac{D_\Pi}{2}\right)}{\Gamma_f\left(\frac{D_\Pi}{2}\right) + \Gamma_D + \Gamma_\gamma}\right). \qquad (4)$$

When resonance overlap is to be taken into account the picket-fence model yields for the width $\Gamma_f(x)$

$$\Gamma_f(x) = \frac{\Gamma_{\Pi c}\Gamma_{\Pi f} D_\Pi}{\Gamma_\Pi D_\Pi} \cdot \frac{\sinh(\pi\Gamma_\Pi/D_\Pi)}{\cosh(\pi\Gamma_\Pi/D_\Pi) - \cos(2\pi x/D_\Pi)} \qquad (5)$$

$$= \frac{C_1}{C_2 - \cos(2\pi x/D_{II})} , \tag{6}$$

where

$$C_1 = \frac{\Gamma_{IK}\Gamma_{II}D_I}{\Gamma_I D_{II}} \sinh(\pi\Gamma_{II}/D_{II}) , \tag{7}$$

and

$$C_2 = \cosh(\pi\Gamma_{II}/D_{II}) . \tag{8}$$

Therefore

$$\int_0^{D_{II}} \frac{\Gamma_f(x)\,dx}{\Gamma_f(x)+\Gamma_D+\Gamma_\gamma}$$

$$= \int_0^{D_{II}} \frac{\dfrac{C_1}{C_2-\cos(2\pi x/D_{II})}}{\dfrac{C_1}{C_2-\cos(2\pi x/D_{II})}+\Gamma_D+\Gamma_\gamma}\,dx$$

$$= \int_0^{D_{II}} \frac{\dfrac{C_1}{\Gamma_D+\Gamma_\gamma}\,dx}{\dfrac{C_1}{\Gamma_D+\Gamma_\gamma}+C_2-\cos(2\pi x/D_{II})} . \tag{9}$$

This can easily be transformed to the form of the known* integral

$$\int_0^{2\pi} \frac{d\varphi}{M-\cos\varphi} = \frac{2\pi}{\sqrt{M^2-1}} \quad \text{for} \quad M>1, \tag{10}$$

*This integral can be found in CRC Handbook of Chemistry and Physics, 62nd edition, edited by Robert C. Weast, Page A-71.

Let $$\varphi = 2\pi x/D_{II} \,, \quad G = \frac{C_1}{\Gamma_D + \Gamma_\gamma} \,.$$

Then $$\int_0^{D_{II}} \frac{\Gamma_f(x)\,dx}{\Gamma_f(x) + \Gamma_D + \Gamma_\gamma}$$

$$= \frac{D_{II} G}{2\pi} \int_0^{2\pi} \frac{d\varphi}{G + C_2 - \cos\varphi}$$

$$= \frac{D_{II} G}{\sqrt{(G + C_2)^2 - 1}}$$

$$= \frac{1}{\sqrt{\left(G + \cosh(\pi \Gamma_{II}/D_{II})\right)^2 - 1}} \,. \qquad (11)$$

where

$$G = \frac{\Gamma_{IIc}\,\Gamma_{IIf}\,D_I \sinh(\pi \Gamma_{II}/D_{II})}{\Gamma_{II} D_{II} (\Gamma_D + \Gamma_\gamma)} \,. \qquad (12)$$

Substuting (2),(3),(4),(10),and (11) into (1),and taking into account fission width fluctuation,one can obtain Equation (15) of Chapter IV.

$$A = \sigma_\gamma D_{II} (P_2 - P_1) \Gamma_\gamma / (\Gamma_\gamma + \Gamma_D) \,,$$

where $$P_1 = \frac{S \Gamma_f(x = D_{II}/2)}{\Gamma_f(x = D_{II}/2) + \Gamma_D + \Gamma_\gamma}$$

and $$P_2 = SG\left((G + \cosh(\pi \Gamma_{II}/D_{II}))^2 - 1\right)^{-1/2} \,.$$